Medical Science Division

MSc by Research in Pharmacology

Surface-Modified Microparticles of Iron Oxide: Biodistribution, Systemic Inflammatory Modulation and MRI Applications in the Early Stages of CNS Inflammation

Shiqing Wang

Green Templeton College

Acknowledgements

I would first like to thank Dr Daniel Anthony for the opportunity to work in his laboratory on such an exciting project, and also for his inspirational supervision. I would also like to thank Prof. Nigel Emptage for his encouragement of my research interests and career development.

I feel deeply grateful to my college advisor, Prof. Derek Jewell, for his endless care and devotion in being a nice mentor. He is not only a patient teacher, but also a wise colleague and a 'kind grandfather' to me. I enjoyed the time with him very much.

I would also like to acknowledge my colleagues, Guillaume Bort and Yvonne Couch, for all their days of hard work in the laboratory. Both were very dedicated individuals and great examples to me.

I would also like to thank Paula Savin, the Academic Administrator in the Department of Pharmacology, for her contributions to all the students, every day.

Last but not least, I would like to embrace my parents for their full support on every decision I have made, and hope I can make them proud in the future.

List of Abbreviations

APP	acute-phase proteins
APR	acute-phase response
BBB	blood-brain barrier
B-CSF	blood-cerebrospinal fluid
CBF	cerebral blood flow
CCI	controlled cortical impact
CCL	chemokine (C-C motif) ligand
CCR	chemokine receptor
cDNA	complementary deoxyribonucleic acid
C/EBP β	CAAT enhancer binding protein beta
CLIO	cross-linked iron oxide
CNS	central nervous system
COX	cyclooxygenase
CRD	cysteine-rich domain
CRP	C-reactive protein
CSF	cerebrospinal fluid
Ct	cycle threshold
CT-1	cardiotrophin-1
CXCL	chemokine (C-X-C motif) ligand
CXCR	chemokine (C-X-C motif) ligand receptor
DC-SIGN	dendritic cell-specific intercellular adhesion molecule-3-grabbing non-integrin
DC-SIGNR	homologue of DC-SIGN
DMSO	dimethyl sulfoxide
DNA	deoxyribonucleic acid
dNTP	deoxyribonucleotide triphosphate
EAE	experimental autoimmune encephalomyelitis

EGFR	epidermal growth factor receptor
ELISA	enzyme-linked immunosorbent assay
ERK	extracellular-signal regulated kinase
ESBP	E-selectin-binding-peptide
ESL-1	E-selectin ligand-1
FDG	^{18}F-fluorodeoxyglucose
FMT	fluorescent molecular tomography
FUT-2	galactoside 2-α-L-fucosyltransferase
FUT-3	α(1,3/1,4)-fucosyltransferase
GAPDH	glyceraldehyde 3-phosphate dehydrogenase
Gd	gadolinium
GlcNAc	N-acetylglucosamine
GLUT1	glucose transporter protein 1
HRP	horseradish peroxidase
HUVEC	human umbilical vein endothelial cells
ICAM	intercellular adhesion molecule
IFN-γ	interferon-γ
JAM	junctional adhesion molecule
JNK	c-Jun N-terminal kinase
KO	knockout
LE^A	Lewis A antigen
LE^B	Lewis B antigen
LE^X	Lewis X antigen
LE^Y	Lewis Y antigen
LIF	leukaemia inhibitory factor
LPS	lipopolysaccharide
mAb	monoclonal antibody

MCAO	middle cerebral artery occlusion
β-MCE	β-mercaptoethanol
MMP9	matrix metalloproteinase 9
MPIO	micron-sized particles of iron oxide
MRI	magnetic resonance imaging
MS	multiple sclerosis
MTT	3-[4,5-dimethylthiazol-2-yl]-2,5 diphenyl tetrazolium bromide
NF-κB	nuclear factor kappa-B
PBS	phosphate-buffered saline
PCR	polymerase chain reaction
PEG	polyethylene glycol
PEGF	poly-(ethylene glycol)-co-fumarate
PEI	polyethylenimine
PET	positron emission tomography
PFA	paraformaldehyde
PLA	polylactic acid
PLA-PEG	polylactic acid-co-polyethylene glycol
PSGL-1	P-selectin glycoprotein ligand-1
PVA	polyvinyl alcohol
PVP	polyvinyl pyrrolidine
RNA	ribonucleic acid
RT	reverse transcription
SAP	serum amyloid P
SEC	size exclusion chromatography
SPR	surface plasmon resonance
sLE^A	sialyl Lewis A
sLE^X	sialyl Lewis X

SPECT	single positron emission computed tomography
SPIO	superparamagnetic particles of iron oxide
TBI	traumatic brain injury
TE	echo time
TGF-β	transforming growth factor-β
TNFα	tumour necrosis factor-α
TR	repetition time
TSPO	translocator protein-18kDa
UPA	urokinase plasminogen activator
USPIO	ultra-small superparamagnetic particles of iron oxide
VCAM-1	vascular cell adhesion molecule-1
VE	vascular endothelial
VEGF	vascular endothelial growth factor
VLA-4	integrin very late antigen-4
WST	water soluble tetrazolium salt
WT	wild-type
ZO-1	zona glomerulosa protein-1

Abstract

Magnetic resonance imaging of central nervous system inflammation in animal models is evolving rapidly due to the continuing development of sophisticated contrast-enhancing agents. Once conjugated with specific functional groups, these contrast-enhancing agents can identify inflamed sites on brain endothelium. However, the potential endogenous ligands that they target and the influence of their physicochemical properties on systemic inflammation are currently not well understood. The aim of this project was to investigate the systemic effect of novel MRI agents, including microparticles of iron oxide (MPIO) coated with Lewis oligosaccharides, carboxylic acids or amines, on the early stages of rodent central nervous system inflammation induced by IL-1β. Lewis A and Lewis B-linked MPIOs (Le^A/Le^B-MPIOs) produced intense MRI signals 4 h after intracranial injection of IL-1β in rats. Prussian blue staining and immunohistochemistry demonstrated unequivocally that Le^A/Le^B-MPIOs selectively bind to endothelial cell-like structures in the rat brain during inflammation. Furthermore, Lewis antigen-coated MPIOs enhanced cerebral neutrophil recruitment by disrupting the integrity of the blood-brain barrier. Investigation of the pharmacological effects of charged MPIOs *in vivo* in CD-1 mice showed that the hepatic and splenic expression of certain pro-inflammatory mediators was suppressed by amine-coated MPIOs (by 40–80%). These positively charged MPIOs also suppressed hepatic neutrophil recruitment, but had no influence on splenic or cerebral neutrophil recruitment, the integrity of the blood-brain barrier, or the cerebral expression of the GLUT1 transporter in mice. Downregulation of the systemic acute-phase response and neutrophil recruitment by amine-coated MPIOs was only observed in IL-1β-injured mice. In conclusion, the findings suggest that Le^A/Le^B-MPIOs enhance MRI contrast through an affinity to as yet unidentified targets on activated endothelium. However, it should be noted that their potential side effects to accelerate the cerebral inflammatory process should be investigated fully before any further clinical applications are considered. It is also noteworthy that the pharmacological role of MPIOs is greatly dependent on their surface charge, with positively charged MPIOs suppressing the early-stage acute-phase response and leukocyte migration under physiological conditions.

Introduction

Vascular inflammation in the central nervous system (CNS) is a key feature of both acute vascular syndromes, such as ischaemic stroke (1–2), and some neurodegenerative diseases, including multiple sclerosis (MS) and Alzheimer's disease (3). The development of effective imaging methods for identifying CNS inflammatory sites during their early stages would be clinically beneficial for patients at future risk from these diseases. Much progress has been made in applying molecular imaging techniques to address this problem. The main focus has been on the key steps involved in the inflammatory cascade, for example, vascular endothelial activation, leukocyte recruitment, extracellular matrix degradation and apoptosis (4). Endothelial activation is a prominent feature characterised by the upregulation of vascular cell adhesion molecule-1 (VCAM-1), intercellular adhesion molecule-1 (ICAM-1), and P-/E-selectin, which promote leukocyte recruitment to the vascular wall and the development of lesions. The initial leukocyte rolling along activated endothelium is mainly due to the interaction between P-selectin and P-selectin glycoprotein ligand-1 (PSGL-1), while firm leukocyte adhesion is mediated by VCAM-1, with the engagement of the integrin very late antigen-4 (VLA-4) (Figure 1) (5). These endovascular adhesion molecules are ideally suited to function as imaging targets for agents designed to reveal the different stages of CNS inflammation. It is interesting to note that peripheral inflammation has been shown to modulate cerebral inflammation though neuroimmune communications (6). At the onset of brain inflammation, inflammatory mediators are secreted into the circulation by astrocytes and microglia, and these mediators subsequently initiate a hepatic acute-phase response (APR) systemically that in turn accelerates leukocyte migration from the lymphoid organs to the CNS. The measurement of cerebral-peripheral immunological communication signals thus provides an accessible method for evaluating the level of brain inflammation. Figure 1 shows

schematically the process of leukocyte adhesion and infiltration across an endothelium that has been activated.

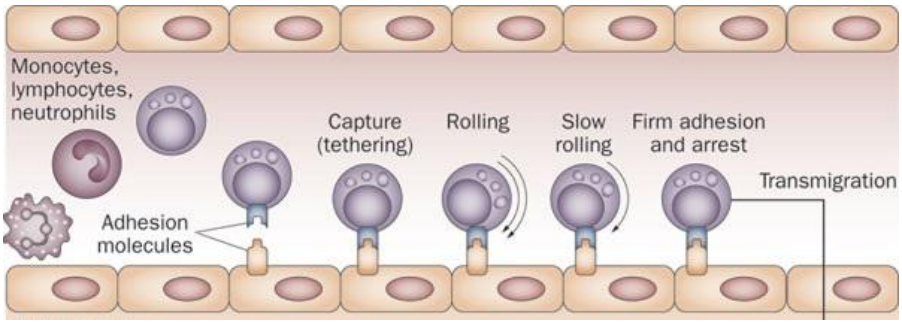

Figure 1. Leukocyte adhesion and infiltration across an activated endothelium.

Circulating leukocytes move towards the activated endothelium and initially are tethered by transient adhesion before rolling along the endothelium, an effect mediated by the upregulation of P-/E-selectin on the endothelial cells. Subsequently, the leukocyte rolling velocity drops dramatically to 5–10 μm/s because of the action of E-selectin and CD18 integrins, respectively. Finally, the leukocytes become firmly adhered when the VLA-4 on their cell surfaces binds to VCAM-1 on the activated endothelium. The leukocytes then transmigrate the endothelium, a process mediated by CD31, vascular endothelial (VE)-cadherin, CD18 and CD47 (adapted from reference 7).

Homeostasis of the CNS is largely maintained within strict limits by specialised mechanisms, both anatomical and immunological, which prevent the unrestricted access of molecules from the general circulation to the brain parenchyma (neurons and astrocytes). These anatomical specializations consist of two barriers: the blood-brain barrier (BBB) and the blood-cerebrospinal fluid (B-CSF) barrier. In both barriers, the endothelial cells are linked by tight junctions, which differ slightly in their morphology (8–9). In particular, the arterioles and capillaries in the brain have continuous tight junctions between individual endothelial cells, while the intercellular junctions are much looser in venules (10). Parenchymal but not

pial vessels are surrounded by astrocyte endfeet to form functional neurovascular units. There is also differential expression of adhesion molecules between blood vessels in different regions of the brain. For example, P- and E-selectin are detected in microvessels of the subarachnoid space but not in the deeper parenchymal vessels (11), implying that vascular beds in the various brain regions may have different immune mechanisms for the initiation of CNS inflammation.

Presently, a number of non-invasive molecular imaging techniques are able to delineate CNS inflammatory sites to determine the efficacy of treatment. These methods include magnetic resonance imaging (MRI), positron emission tomography (PET), single positron emission computed tomography (SPECT), and fluorescent molecular tomography (FMT). Nuclear imaging techniques allow quantitative measurement of inflamed sites, with PET having a higher temporal resolution and sensitivity than SPECT. For example, PET has revealed that ^{18}F-fluorodeoxyglucose (FDG) accumulates (in the nanomolar to picomolar range) in macrophage-rich atherosclerotic plaques (12–13). However, PET and SPECT remain limited by their poor spatial resolution, high expense, and the need to expose patients to ionising radiation. MRI has certain advantages over PET, in that it can detect early CNS inflammation, and provide high spatial and temporal resolution images with excellent tissue contrast and minimal exposure to ionising radiation. As a part of the latest methodological advances, nanoparticles '*carrying*' substantial payloads of amphipathic gadolinium (Gd) chelates have been added to liposomes (14) or perfluorocarbon lipid emulsions (15) to enhance the sensitivity of MRI detection. However, one potential drawback is that Gd chelates are rapidly cleared from the circulation by the kidneys, and there is an increased risk of nephrogenic systemic fibrosis in patients with renal impairment (16–17). Recently, this potential drawback has been overcome by utilising iron oxide particles as novel MRI contrast agents (Figure 2). These particles consist of iron oxide cores coated with surface complexing

agents such as dextran or polyethylene glycol, and are classified by size as ultra-small superparamagnetic particles of iron oxide (USPIO, 20–50 nm), superparamagnetic particles of iron oxide (SPIO, 50–250 nm), and micron-sized particles of iron oxide (MPIO, 0.5–5 μm). In addition to their superior sensitivity compared with Gd, iron oxide particles are cleared by methods other than renal elimination, making them superior for potential CNS diagnostic applications (18). For example, the liver provides the critical function of catabolism and biliary excretion of particles, making it important to eliminate iron-oxide particles by hepatocyte-mediated phagocytosis (19). The liver has been reported to efficiently capture and eliminate USPIOs, with no research on MPIOs in the liver metabolism yet.

A number of superparamagnetic iron oxide agents have been approved for use in CNS imaging of humans, such as ferumoxtran-10 (20-21), SHU555C (22) and ferumoxytol (23). Preliminary studies using these iron oxide particles have not revealed any significant acute or medium-term toxicity (24). In contrast to Gd chelates, which have been used for the imaging of BBB disruption and alterations in cerebral blood flow (CBF), phagocytosed non-coated iron oxide particles have mainly been employed to study the trafficking of macrophages or other leukocytes. Prominent differences have been observed in the MRI enhancement patterns between iron oxide particles and Gd; for example, during the first MS relapse, numerous USPIO-enhancing areas were found not to show any Gd uptake by MRI (25–26). The actual distribution of different iron oxide particles is combinatively decided by their diffusion across the BBB, adhesion to non-inflamed/inflamed vessel walls, and the rates of their uptake by monocytes/macrophages and potential opsonisation, which will activate lymphocytes. These pharmacological features are dependent on the hydrodynamic radius and surface properties of the particles, which are precisely modified to optimise imaging during the early stages of CNS inflammation or brain tumour development (27).

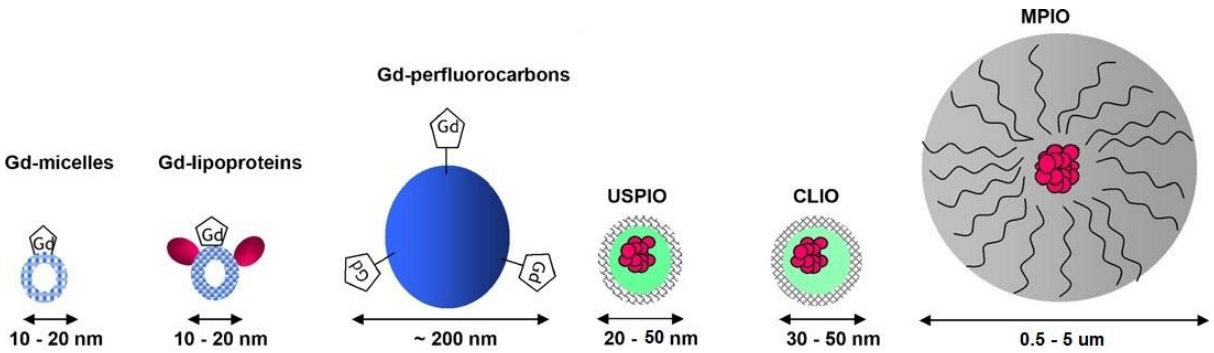

Figure 2. Novel MRI contrast agents. Gd, gadolinium; CLIO, cross-linked iron oxide; MPIO, micron-sized particles of iron oxide; USPIO, ultra-small superparamagnetic particles of iron oxide.

The novel MRI contrast agents can carry significant amounts of Gd chelates or iron oxide in the form of decorated liposomes, polymer micelles, or nano-/micron-sized particles. Gd chelates usually decorate the surface of the carrier to ensure the contrast-generating interaction between Gd chelates and local water molecules, while iron oxide is usually embedded within polymer shells to ensure biocompatibility (28). The influence of particle size on blood clearance and phagocytosis has been studied for more than two decades (29). Among the iron particle subtypes, MPIOs are particularly promising for endothelial cell-specific molecular imaging, for several reasons. First, due to their micrometre size range, MPIOs retain endovascular specificity without showing the disadvantages of non-specific macrophage uptake or vascular egress (30); in contrast, USPIOs are avidly taken up by most leukocytes, including circulating and residential monocytes/macrophages, mononuclear T cells, reactive microglia and even dendritic cells. Second, although USPIOs have shown promise in the imaging of macrophage-rich atherosclerotic plaques (31) and the tracking of circulating macrophages (32), their ability to precisely target inflamed sites within blood brain vessels has being questioned. MPIOs have a very short half-life in the circulation of 45–100 s (33–34), producing a high target-to-background ratio and allowing MRI to start immediately after injection. This advantage contrasts with the properties of USPIOs, which

require a blood clearance time of ≥ 24 h, and show a measurable T_1-weighted signal enhancement that starts 4–6 h after injection (23). Third, USPIOs slowly leak across the BBB (through unknown mechanisms), while preliminary data demonstrate that iron oxide particles larger than USPIOs do not leak across the BBB, 4 h after injection (35). Fourth, MPIOs create potent hypointense MRI contrast effects on T_2-weighted images, thereby enhancing the detection sensitivity for endothelial molecular targets of low abundance. It is also noteworthy that alterations in the surface properties of iron oxide particles are of great importance for modifying the imaging and pharmacological effects of these contrast agents. Biocompatible coatings such as carboxydextran are beneficial for particle phagocytosis and can be used for signal enhancement in MR-related imaging (36). Other coating materials, including amphiphilic polylactic acid (PLA), polylactic acid-co-polyethylene glycol (PLA-PEG) and polystyrene, are also suitable for *in vivo* tests, and these chemicals can be linked to antibodies or carbohydrate analogues for molecular targeting. Surface charge may be another critical factor that influences particle distribution. For example, the ionic SPIOs have a significantly higher cellular uptake compared with non-ionic SPIOs of a similar size (37). Amines and carboxylic acids (with anionic and cationic physiological actions, respectively) have been designed for embolisation or implantation to induce specific cell responses, in regard to cytokine production (38) and apoptosis (39). It has been demonstrated that cationic carriers bind non-specifically to anionic cell surfaces through electrostatic interactions (40). Furthermore, the existence of cationic substitution not only stimulates cytokine release from cultured macrophages, but also induces macrophage apoptosis and neutrophil activation (41–42), indicating that cationic carriers could be potential agents to enhance MRI contrast as well as produce modulatory effects on the progression of CNS inflammation. It should be emphasized that all studies of the pharmacological effects of surface charge on microparticles or nanoparticles have been undertaken using *in vitro* experiments, suggesting that it may be

necessary to inject charged MPIOs intravenously to explore inflammatory processes more deeply.

Revealing the earlier molecular changes, rather than the later structural changes, in brain vascular inflammation has become the main research priority when developing novel imaging tools. New endovascular molecular MRI contrast agents, formed by covalently conjugating residues on the surface of iron oxide particles to peptide or carbohydrate ligands, have recently been characterised (Table 1) (43–54). These ligands are generally monoclonal antibodies (mAb), single-chain antibody fragments or saccharide ligands that bind to adhesion molecules that are rapidly upregulated during endothelial activation. In particular, antibodies to VCAM-1, ICAM-1 and selectins have been extensively applied to improve the binding specificity of iron oxide particles to inflamed sites, in order to facilitate precise imaging. For *in vitro* studies, the polydextran coating of USPIOs has been conjugated to both E-selectin-binding peptide (ESBP) and a near-infrared indocyanine fluorophore (Cy5.5) to visualize their adhesion to activated human umbilical vein endothelial cells (HUVEC) (55). MPIOs have also been cross-linked to mAb that targets VCAM-1, and these have been found to bind to activated mouse endothelial cell lines (56). Promising *in vivo* MRI results have been obtained using VCAM-1-mAb-linked MPIOs to detect inflammatory processes associated with cerebral ischaemia (57), MS (56), brain metastases (58) and seizure-induced inflammation (59) in corresponding animal models. The large ‘payload’ of iron and the low constitutive expression of VCAM-1 have permitted VCAM-1-mAb-conjugated MPIOs to be used as early and sensitive markers of inflamed sites that cannot be detected using Gd chelates (57), potentially allowing for the early diagnosis of CNS inflammation. By cross-linking E-/P-selectin antibody fragments to iron oxide particles, contrast agents other than VCAM-1-mAb-conjugated MPIOs have been developed for targeted imaging, and these are presently being tested in animal models of vascular inflammation (60).

Antibodies can be prepared in large quantities by solid-phase synthesis, but at a much higher expense compared to the production of carbohydrates. Considering this cost implication, the glycans that naturally exist in the recognition site of selectin receptors can be conjugated to MPIOs to enable quantitative analysis of selectin expression along the course of blood vessels. Previous investigations have assigned E-/P-selectin binding activity to Lewis carbohydrate motifs, including sialyl Lewis A (sLe^A), sialyl Lewis X (sLe^X), and an internally fucosylated sLe^X isomer called VIM-2, on the surface of selectin ligands such as L-selectin, E-selectin ligand-1 (ESL-1) and PSGL-1 (61–62). These O-glycans are synthesized by selective glycosyltransferases and fucosyltransferases, and are essential to the targeting of E-/P-selectin on activated endothelium. In addition, a sulphated Lewis carbohydrate, 6-sulfo sialyl Lewis X (6-sulfo sLe^X), on endothelial cells is regarded as the L-selectin binding motif in lymphocyte homing. During inflammation, the expression of these Lewis motifs is greatly upregulated by cytokine stimulation (63), and plays a critical role in the recruitment of neutrophils, monocytes and lymphocytes to lesion sites.

The assembly of Lewis carbohydrates involves the sequential addition of specific monosaccharides onto terminal saccharide precursors on the glycoproteins. There are four Lewis antigens, termed Lewis A (Le^A), Lewis B (Le^B), Lewis X (Le^X) and Lewis Y (Le^Y), respectively. All of these are tetrasaccharides synthesized by the addition of fucose to the central N-acetylglucosamine (GlcNAc) of the core structure, through the action of diverse fucosyltransferases. Le^A and Le^X are produced if α(1,3/1,4)-fucosyltransferase (FUT-3) is involved, while Le^B and Le^Y are synthesized by galactoside 2-α-L-fucosyltransferase (FUT-2). According to steric hindrance studies, only Le^A and Le^X can be further sialylated to form sLe^A and sLe^X, respectively. In addition, due to their structural similarity, Le^A and Le^B are usually defined as type I Lewis carbohydrates, while Le^B and Le^Y are recognized as type II Lewis carbohydrates (64).

Table 1. Targeted iron oxide particles in development for molecular imaging.

Conjugated molecule on the surface	Biological target	Ref.
Wheat germ agglutinin	Axon terminals	(43)
Transferrin protein	Transferrin receptors	(44)
Anti-myosin mAb	Myocardial infarction	(45)
Aβ 1–40	Amyloid plague	(46)
Neuroblastoma-specific cell surface antigen	Neuroblastoma cancer	(47)
Anti-Her2/neu	Her2/neu receptor on tumor cells	(48)
Succinylated polylysine	Lymph nodes	(49)
Anti-EGFR	EGFR in carcinoma	(50)
Anti-P-/E-selectin	Activated endothelium	(51)
Annexin V	Apoptotic cells	(52)
Anti-VCAM-1	Activated endothelium	(53)
Sialyl Lewis	Activated endothelium	(54)

mAB, monoclonal antibody; EGFR, epidermal growth factor receptor; VCAM-1, vascular cell adhesion molecule-1.

Under normal conditions, the synthesis of Lewis antigens occurs predominantly in epithelial cells. Subsequently, these glycans are carried by glycolipids into the circulation, where they are adsorbed by erythrocytes (65). At the onset of inflammation, activated leukocytes can also express these Lewis antigens on their surfaces (63).

The sialylated Lewis glycans show more promise than antibodies for the targeting of selectin upregulation, and have been conjugated to contrast agents for the imaging of selectin expression in animal disease models (54). Previous attempts to detect selectin expression by antibodies *in vivo* have failed (66) or shown only limited contrast enhancement (67–69); to

date, there have been no applications in validated models of brain inflammatory disorders. The first use of sialylated Lewis glycans in molecular MRI involved their cross-linking to Gd-based nanoparticles for the detection of early cerebral endothelial activation (67). Subsequently, liposomes bound to sLe^X with encapsulated fluorescent markers were shown to successfully co-localize with E-selectin in a mouse model of arthritis (70). Recently, iron oxide particles coated with sLe^X, containing about 10^5 to 10^7 glycans per USPIO, have been developed and tested in both *in vitro* and *in vivo* experiments (54). The sLe^X-USPIOs showed strong and selective binding to an E-selectin-F_c chimeric protein in an *in vitro* binding assay, and also provided excellent MRI contrast in animal models of MS and stroke, before any breakdown in the BBB was detected using Gd chelates. Therefore, sLe^X-USPIOs and other carbohydrate-linked iron oxide particles have great potential for the early detection of several neuropathologies, including MS, stroke, multi-infarct dementia and Parkinson's disease. In particular, when the advantages of MPIOs are taken into consideration (*vide supra*), glycan-coated MPIOs may be especially promising and worthy of investigation for their contrast enhancement properties.

While the pharmacological roles of sialyl Lewis antigens have been thoroughly investigated, there is a paucity of data concerning the expression and function of unsialylated and disialylated Lewis glycans *in vivo*. This MSc project was devised based on preliminary data from my host laboratory, which demonstrated for the first time that MPIOs coated with unsialylated Lewis antigens could enhance the contrast of endovascular inflammation imaging in a similar manner to sLe^X-MPIOs (Figure 3). Briefly, type I Le^A- and Le^B-coated MPIOs (Le^A/Le^B-MPIOs), rather than type II Le^X- and Le^Y-coated MPIOs (Le^X/Le^Y-MPIOs), were found to co-localize at inflamed sites after acute inflammation was artificially induced. Four hours after the intracranial injection of interleukin-1β (IL-1β) to the ipsilateral hemisphere, the 4 types of Lewis glycan-conjugated MPIOs were injected intravenously and

their course followed by MRI scanning to study their distribution. The results strongly suggested that unsialylated Lewis antigens target inflamed sites, but utilise different mechanisms to sialylated antigens.

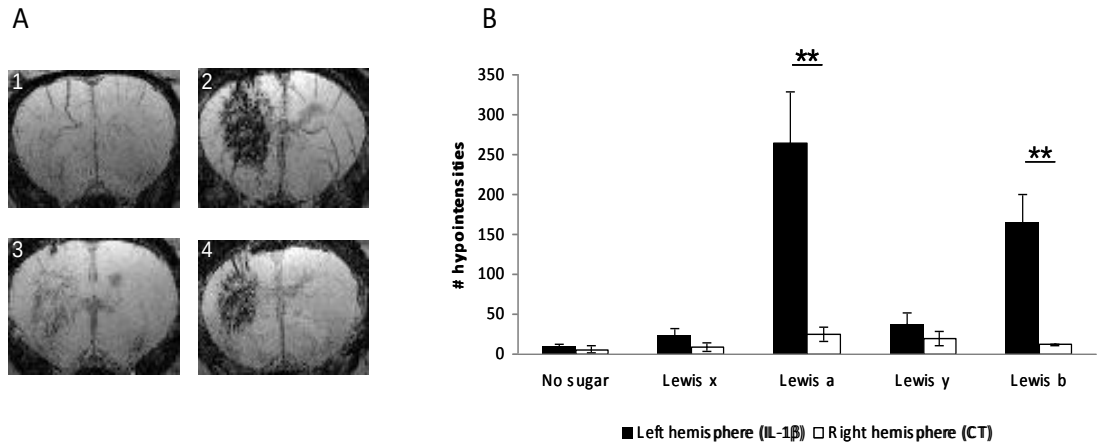

Figure 3. MRI contrast enhancement in the IL-1β-injured rat brain after intravenous injection of Le^A/Le^B-MPIOs. A: Minimum intensity projections obtained from *in vivo* MRI of the left hemisphere of the rat brain, after intracerebral injection of IL-1β, using MPIOs coated with Le^X (1), Le^A (2), Le^Y (3) and Le^B (4). n = 4 for IL-1β ic + Le^A-MPIO iv, n = 3 for other group. The images shown are representative of the results in each group. B: quantification of the black pixels in the minimum intensity projections of the left (IL-1β) and right (control) brain hemispheres (s). The error bars represent the mean ± standard error of the mean (SEM). **P < 0.01. Authorized by Guillaume Bort.

Much remains to be elucidated about the mechanisms underlying signal enhancement by unsialylated Lewis antigens. First, it is still unknown whether Le^A/Le^B-MPIOs adhere to activated endothelium or enter into the brain parenchyma by monocyte/macrophage infiltration following their injection into the blood circulation. The use of Prussian blue staining after pre-treatment facilitates the study of the mechanism of contrast enhancement by allowing the distributional pattern of these coated MPIOs to be followed (71). Second, it is

vital to determine the specific molecular targets of unsialylated type I Lewis carbohydrates. The only molecule on the leukocyte surface known to exhibit binding affinity with unsialylated Lewis antigens are the transmembrane lectin receptors, termed dendritic cell-specific intercellular adhesion molecule-3-grabbing non-integrin (DC-SIGN), and its homolog, DC-SIGNR (72). Although DC-SIGN is expressed strictly on dendritic cells, DC-SIGNR is constitutively expressed on the endothelial cells of the liver, lymph nodes, and placental tissue (73), making it a probable target of unsialylated Lewis glycans. The cysteine-rich domains (CRDs) of both DC-SIGN and DC-SIGNR recognize all four unsialylated Lewis carbohydrates on viruses and leukocytes *in vivo*, suggesting that DC-SIGN/DC-SIGNRs may contain CRDs with a specific binding affinity for Le^A and Le^B. Third, despite the short clearance time of MPIOs, the influence of these unsialylated Lewis residues on the inflammatory process should also be studied systemically to avoid potential adverse effects; in other words, there should be a focus on peripheral as well as CNS inflammation.

Systemic inflammation has been recognized as an essential component of the cerebral inflammatory process. In response to CNS injury, the hepatic expression of almost a thousand genes is changed significantly (74). This modulation, called APR, is mediated either by the secretion of IL-1β and tumour necrosis factor-α (TNFα) from microglia into the circulation or by the activation of cholinergic vagal efferents that innervate the liver (75). The hepatic response incorporates the release of cytokines, chemokines and other acute-phase proteins (APP), such as C-reactive protein (CRP) and serum amyloid P (SAP) (74), which leads to subsequent leukocyte recruitment to the peripheral and cerebral inflamed sites. For example, there is a hepatic chemokine response within 2 h of spinal cord injury, causing leukocyte influx into the liver, lungs and kidneys (76–78). This leukocyte recruitment contributes to the damage caused to these organs (79). Damage from the APR occurs not only in peripheral

organs but also acts to amplify the focal injury response of the brain. Thus, paradoxically, CNS inflammation should be considered as a systemic pathological process (74, 80).

Various animal models have been developed to mimic the CNS inflammatory changes in MS, ischaemic stroke, spinal injury and brain metastases (81–82). In addition, the intracranial release of a single cytokine in the ipsilateral hemisphere can produce observable temporal effects on systemic inflammation. There are two established methods to elicit cytokine secretion experimentally: one-bolus injection of cytokine directly into the striatum to mimic acute brain injury; or intrastriatal injection of a recombinant and replication-deficient adenovirus vector to cause the chronic expression of cytokines in the brain. IL-1β and TNFα are frequently used, in accordance with their importance in the APR. IL-1β has been shown to play a pivotal role in the exacerbation of acute neurodegeneration caused by ischaemia, head trauma or stroke, and has been implicated in the pathology of MS, Alzheimer's disease and other chronic CNS inflammatory conditions (83–85). The IL-1β level in the CSF of MS patients has been found to correlate with the disease severity and pathological progression (86–87). Moreover, blocking IL-1β successfully reduces neuronal loss and inflammation (88–89). Similarly, TNFα has been reported to contribute to the pathology of MS, ischaemic stroke and Parkinson's disease (90–92). Overexpression of TNFα leads to demyelinating disease, while neutralization of TNFα with antibodies is protective in animal models of MS (93–94). Although IL-1β and TNFα have many similarities, their patterns of leukocyte recruitment differ (71, 95–96). Intracranial injection of IL-1β leads to localized neutrophil recruitment, whereas microinjection of TNFα into the brain gives rise to a distinct pattern characterized by the recruitment of T cells and monocytes. Moreover, different inflammatory responses occur following acute and chronic cytokine release. An intracranial injection of IL-1β into the brain parenchyma does not overtly lead to damage of the integrity of the BBB, whereas 8 days of continuous adenoviral expression of

IL-1β in the brain produces a marked breakdown of the BBB, which is similar to the BBB disruption observed after chronic expression of TNFα in the striatum (71, 97). Therefore, it is of great importance to select a simplified inflammatory model at the onset of the project to avoid the difficulties associated with studying too many variables.

The aims of the present study were to obtain further insights into the pharmacological effects and relevant mechanisms of two MPIO subtypes: MPIOs coated with unsialylated Lewis antigens, and MPIOs coated with amines or carboxylic acids, which behave as charged microparticles under physiological conditions. Acute brain inflammation was induced by intracranial injection of IL-1β or TNFα, thus providing the simplest possible acute inflammatory model. In the first part of the study, Prussian blue staining and immunostaining were utilised to determine the distributions of these particles in the brain parenchyma, and comparisons were made with corresponding MRI data. Second, the integrity of the BBB and cerebral leukocyte recruitment were investigated to determine whether the inflammatory processes were affected by MPIO injection. Finally, the systemic responses to the charged MPIOs were evaluated by measuring neutrophil recruitment and APP expression levels in the liver and spleen. At the organ-based level, it has recently been discovered that MPIOs are rapidly sequestered by the liver and spleen partly through endocytosis mediated by macrophages (termed Kupffer cells in the liver) (98); this is similar to reticuloendothelial system-based USPIO clearance (99–100). Since the liver dominates the immune crosstalk between the periphery and the brain (74, 101), it is hypothesized that circulating MPIOs might affect systemic inflammation by modulating hepatic or splenic inflammatory responses. Thus, this project will provide important information on the systemic pharmacological roles of certain coating molecules.

In general, the purpose of this MSc project and further investigations after my MSc study can be concluded as below:

1) Observe the distribution of coated MPIOs by MRI and immunostaining data (finished);
2) Clarify the mechanism of specialized distribution in cellular and molecular level (unfinished for further investigation);
3) Measure the systemic inflammatory response of coated MPIOs in both cellular and molecular levels (finished).

Materials and Methods

Synthesis and preparation of coated MPIOs

The amine-coated MPIOs (amine-MPIOs) and carboxylic acid-coated MPIOs (carboxylic-MPIOs) were obtained commercially from NanoLink. The Lewis antigen-coated MPIOs were synthesized by adding Lewis glycans to amine-MPIOs, as follows: 5.8 mg of magnetically washed amine-MPIOs (3 × washing through DynaMag in 0.1 M $NaHCO_3$ buffer, pH 8) was suspended in $NaHCO_3$ buffer (Sigma Aldrich; 100 mM $NaHCO_3$, 0.5 mL, pH 8). The synthesized Lewis glycans (from the Department of Chemistry, Oxford University) were dissolved in $NaHCO_3$ buffer (100 mM $NaHCO_3$, 0.5 mL, pH 8) and then mixed with the solution of amine-MPIOs. The mixture was shaken at room temperature for 15 h. Subsequently, the Lewis-antigen-coated MPIOs were washed with water (3 × 1 mL), dialysed against water, and finally stored in water at 4 ºC. The efficiency of particle loading was measured using the fluoroescamine assay, in which fluoroescamine (Sigma Aldrich; 50 µL in dimethyl sulfoxide [DMSO]) was incubated with MPIO solution for 10 min before measurement of the fluorescence intensity (PerkinElmer; λ_{Ex}: 405 nm, λ_{Em}: 460 nm). After obtaining the conversion rate of particle loading (A%), the coated Lewis antigens per MPIO could be calculated as (based on the following information from the manufacturer: 2.76×10^9 MPIOs per mg of MPIO; 44.5 nmol amino groups per mg of MPIO before linkage; the MPIO density here was re-confirmed using a hemocytometer (Millipore)):

$$\text{Lewis antigen/MPIO} = (44.5 \times 10^{-9}) \times (6.02 \times 10^{23}) \div (2.76 \times 10^{9}) \times (1\text{-A\%})$$

Furthermore, the surface density of the Lewis antigens could also be estimated after knowing the MPIO diameter (730nm) from the manufacturer:

$$\text{Surface density of Lewis antigen (oligosaccharides/nm}^2) = \text{Lewis antigen/MPIO} \div (4 \times 3.14 \times 730^2)$$

Before injection into the experimental animals, all types of MPIO were magnetically washed, dialysed against ddH_2O (3 × 1 mL), and exposed to ultraviolet radiation for 20 min.

Animal model of cytokine-induced brain injury

All procedures involving animals in this project were performed using methods approved by the United Kingdom Home Office in accordance with The Animals (Scientific Procedures) Act (1986). Male Wistar rats and male CD-1 mice (4 weeks old; supplied with food and water *ad libitum*) were anaesthetised with isoflurane (2.0–2.5% in 60% N_2: 40% O_2), positioned in a stereotaxic frame, and viewed using a Wild M650 operating microscope (Leica). For cytokine-induced acute inflammation, 10 ng of IL-1β or TNFα was injected into the left striatum (stereotaxic coordinates for rat: anterior, 1 mm; lateral, 3 mm; depth, 3.5 mm; stereotaxic coordinates for mice: anterior, 0.5 mm; lateral, 2 mm; depth, 2.5 mm; co-ordinated from the bregma). After washing with sterile saline, coated MPIOs were injected intravenously into the tail vein (4 mg Fe/kg) at selected time points after cytokine injection; subsequently, MRI scanning, immunostaining of tissues and RNA extraction were carried out. For MRI scanning and tissue immunostaining, rats and mice were injected with coated MPIOs at time T = 4 h, MRI-scanned 5 min after the MPIO injection, and finally terminally anesthetised at T = 5 h. For the RNA extraction, mice were injected with coated MPIOs at the same time (T = 0 h) as the cytokine injection, and then terminally anesthetised at T = 4 h. Terminal anaesthesia was completed by an intraperitoneal injection of 200 uL (mice) or 500 uL (rats) phenobarbital (Sigma Aldrich).

MRI scanning and analysis of MRI data

All MRI experiments and subsequent data analysis were carried out by collaborators in the Department of Chemistry, Oxford University. In general, images were acquired using a

7-Tesla horizontal-bore magnet with a Varian Inova spectrometer (Varian). A T_2^*-weighted 3D gradient-echo dataset encompassing the entire brain was acquired, using the following parameters: flip angle, 11°; repetition time (TR), 25 ms; echo time (TE), 10 ms; matrix size, 350 × 192 × 192; and field of view, 4.2 × 3.07 × 3.07 cm. The total acquisition time was approximately 1 h. The midpoint of the acquisition was 4.5 ± 0.5 h after the intracranial injection of IL-1β or saline. Data were zero-filled to 350 × 256 × 256 and reconstructed off-line, with a final isotropic voxel size of 120 μm^3. ImageJ software was used to analyse the data. Minimum intensity projections were performed on slices at the injection site. Regions of interest (ROIs) that contained the entire hemisphere were drawn in each section to create pixel intensity histograms; the ROIs contained both hemispheres for the experiments involving systemic injection of lipopolysaccharide (LPS). The signal intensity values were then normalized to the right cortex (signal intensity value = [signal intensity of brain hemisphere]/[signal intensity of right cortex] × 100). The number of pixels in the brain hemisphere below the minimum normalized signal intensity threshold was summated and reported as hypointensities.

Slice preparation

A 10-mL volume of heparinised saline (Sigma Aldrich; 5000 Units/L) and 10 mL of 4% paraformaldehyde (PFA; Fisher Scientific) were sequentially perfused into the left ventricle of a terminated rat or mouse. After perfusion with PFA, the selected organs were embedded in an OCT matrix and snap frozen, with slices collected serially at a thickness of 10 µm using a CM 1850 cryostat (Leica) at a temperature of -18 °C. Specifically, brain slices were collected from anterior to posterior, starting at anterior 2 mm (for rat) or anterior 1.5 mm (for mice), co-ordinated from the bregma. All slices were placed in phosphate-buffered

saline (PBS; Fisher Scientific), to wash out the OCT matrix, before they were dried at room temperature.

Histology

All slices were initially incubated for 20 min with 1% hydrogen peroxide in methanol to eliminate the activity of endogenous peroxidase. The slices were then placed on sequenza clips and blocked with 10% serum (the serum subtype was dependent on the secondary antibodies used later) in PBS for 1 h. Following this, the brain slices were incubated with primary antibodies, while the liver and spleen slices were first treated with avidin (Vector; 1:20 in PBS, 20 min at room temperature) and biotin (Vector; 1:20 in PBS, 20 min at room temperature) before incubation with antibody, in order to block endogenous biotin. For all immunohistochemistry experiments, with the exception of IgG staining, the sections were incubated with anti-neutrophil (horse polyclonal, 1:1000 in PBS, 2 h), anti-Iba-1 (goat monoclonal, 1:500 in PBS, overnight; Abcam) or anti-GLUT-1 (rabbit monoclonal, 1:200 in PBS, overnight; Calbiochem) primary antibodies for the detection of neutrophils, activated microglia/macrophages or brain endothelial cells, respectively. Corresponding biotinylated secondary antibodies to IgG were used, together with the Vectastain ABC-AP kit (Vector), for detection of the primary antibodies, before counterstaining with cresyl violet. For IgG staining, the secondary IgG antibodies were incubated with the sections directly, without the addition of any primary antibodies. For Prussian blue staining, sections were pre-treated with methanol for 15 min to uncoat the polystyrene on the surface of the MPIOs, and this was followed by a 1-h incubation with Prussian blue stain (Sigma Aldrich), and subsequent nuclear fast red counterstaining (Sigma Aldrich; 2 min). Images were captured with a light microscope (Leica) and analysed using ImageJ software. For the quantification of staining

results, 5 fields (within the striatum for brain slices) under microscopic views were randomly chosen to get the target cell counted and the cell number averaged for results from one slice.

RNA extraction

After intracardiac perfusion with ice-cold heparinised saline (5000 units/L), approximately 10 mg each of liver and spleen tissue was collected from terminated mice and snap frozen on dry ice for subsequent RNA extraction. RNA was extracted using a QIAGEN RNeasy Mini Kit, following the instructions provided by the manufacturer. Briefly, tissue samples were homogenized in lysis buffer containing 1% β-mercaptoethanol (β-MCE), and then passed through a QIAshredder mini spin column to shear genomic DNA. RNA was then precipitated from the homogenate using 70% ethanol, passed through an RNeasy spin column and washed. After elution by 25-µL of RNase free water, the quality and quantity of total RNA was analysed using a NanoDrop 1000 Spectrophotometer (Thermo).

Conversion to cDNA

50 ng total RNA was added to a reverse transcription (RT) reaction (total volume, 20 µL) containing dNTPs, RT buffer, random primers, RT enzyme, RNase inhibitor and DNase/RNase free water (all included with the RT kit; Applied Biosystems). All reagents were thoroughly mixed and stored on ice. After running reactions according to the manufacturer's instructions, the final solution was diluted to a cDNA concentration of 5 ng/µL and analysed using a NanoDrop 1000 Spectrophotometer (Thermo).

Quantitative real-time polymerase chain reaction

Real-time quantitative polymerase chain reaction (PCR) was run against a standard curve to analyse the relative ratio of the target gene to the reference gene. Gene-specific

primer pairs and cycle-threshold (Ct) standard curves were generated by Primerdesign, in which the Ct levels were inversely proportional to the amounts of target DNA sequence in the samples. cDNA was added to the mastermix containing SYBR-green dye, and run on a Roche 480 Cycler System. Glyceraldehyde 3-phosphate dehydrogenase (GAPDH) was used as the reference gene for calculating the relative expression of the target gene. The gradient of each standard curve represented the replicating efficiency of each primer when running a series of diluted cDNA templates (these cDNA templates were the mixture of all cDNA samples, to make sure that the standard curve is effective in extrapolating the expression in target samples). For the calculation, the expression of each gene (including the reference gene) in the sample was obtained using their standard curves, then the ratio of target gene expression to reference gene expression is used to compare with the data from other samples.

Statistical analysis

Statistical analysis was performed using Prism software. Data are presented as the mean ± standard deviation (SD) or standard error of the mean (SEM). Comparisons were made using Student's *t*-test. A P value < 0.05 was taken to indicate statistical significance.

Results

Study of the distribution of coated MPIOs in the brain

Four subtypes of Lewis oligosaccharides, namely Le^A, Le^B, Le^X and Le^Y, were attached separately to the surface of amine-MPIOs; among these, both Le^A and Le^B had a unique type I (Galβ1,2GlcNAcβ1-R) structure. Determination, by fluorescamine assay, of the efficiency of oligosaccharide loading onto the particle surface demonstrated that conjugation of about 80% of the amino groups with Lewis glycans was achieved (Table 2). This efficiency corresponds to approximately 7.4–7.9 × 10^6 oligosaccharides per particle and a

local density of 4.4–4.7 oligosaccharides per nm^2. Previous data from my host laboratory had indicated that only Le^A/Le^B-MPIOs produced intense signals in MRI scans of rat brains with acute injury induced by IL-1β (Figure 3). To determine the spatial distribution of the coated MPIOs, it was necessary to use staining techniques to visualize them more precisely in brain tissue. To achieve this, the same Wistar rats used for MRI scanning were terminally anaesthetized at T = 5 h for tissue staining. Prussian blue, counterstained with nuclear fast red, was applied to detect iron oxide particles (102). After pre-treatment with methanol to dissolve the polystyrene coat, only a few spots of Prussian blue staining were found in the ipsilateral striatum where Le^X/Le^Y-MPIOs had been injected, whereas more pronounced staining was observed after the injection of Le^A/Le^B-MPIOs (Figure 4A); these observations correlated well with the MRI scans of each rat brain. Moreover, only Le^A/Le^B-MPIOs co-localized with endothelium-like structures (Figure 4B–C). Only very low numbers of Le^X/Le^Y-MPIOs were found, scattered in the brain parenchyma with no discernable specific pattern (Figure 4D–E).

Table 2. Loading efficiency of unsialyated Lewis glycans on the surface of amine-MPIOs.

Loading property	Lewis A	Lewis B	Lewis X	Lewis Y
Conversion (%)	76.2 ± 10.3	77.6, 82.2	80.1, 82.1	78.6
Oligosaccharides/MPIO ($\times 10^6$)	7.40 ± 1.00	7.32, 8.18	7.78, 7.96	7.63
Oligosaccharides/nm^2	4.42 ± 0.60	4.37, 4.91	4.64, 4.76	4.56

The conversion of the amino groups on the surface of amine-MPIOs was determined by fluorescamine assay. The density of oligosaccharides per MPIO or per nm^2 was based on supplier information (2.76×10^9 MPIOs per mg of MPIO; 44.5 nmol amino groups per mg of MPIO; and an MPIO diameter of 730 nm). The results are presented as the mean ± standard deviation for Le^A-MPIOs ($n = 4$), Le^B-MPIOs ($n = 2$) and Le^X-MPIOs ($n = 2$); $n = 1$ for Le^Y-MPIOs.

The effect of Le^A-MPIOs on MRI contrast was also tested using other rat models of acute brain injury. Intracranial TNFα injection and intravenous LPS injection are considered, along with IL-1β-mediated brain injury, to be among the simplest methods for artificially inducing acute brain inflammation; hence, these approaches were used. In these experiments, Lewis antigen-coated MPIOs were injected intravenously at T = 4 h after TNFα or LPS injection, and this was followed by MRI scanning and terminal anaesthesia. It has been shown previously by my host laboratory that Le^A-MPIOs can also increase the MRI contrast in TNFα- or LPS-activated brains, evident as increased intensity projections from TNFα-activated ipsilateral striatum or LPS-activated brain blood vessels (Figure 5A–B). In the present study, using Prussian blue staining, an enhanced and specific distribution of Le^A-MPIOs was observed in TNFα-injured striatum in accordance with the MRI results (Figure 5C–D). After intravenous injection of LPS in rats, Prussian blue staining was rarely observed in the striatum (Figure 5E); this result corresponds well with the MRI findings that the intensity projections were found mainly in cortical vessels (Figure 5A).

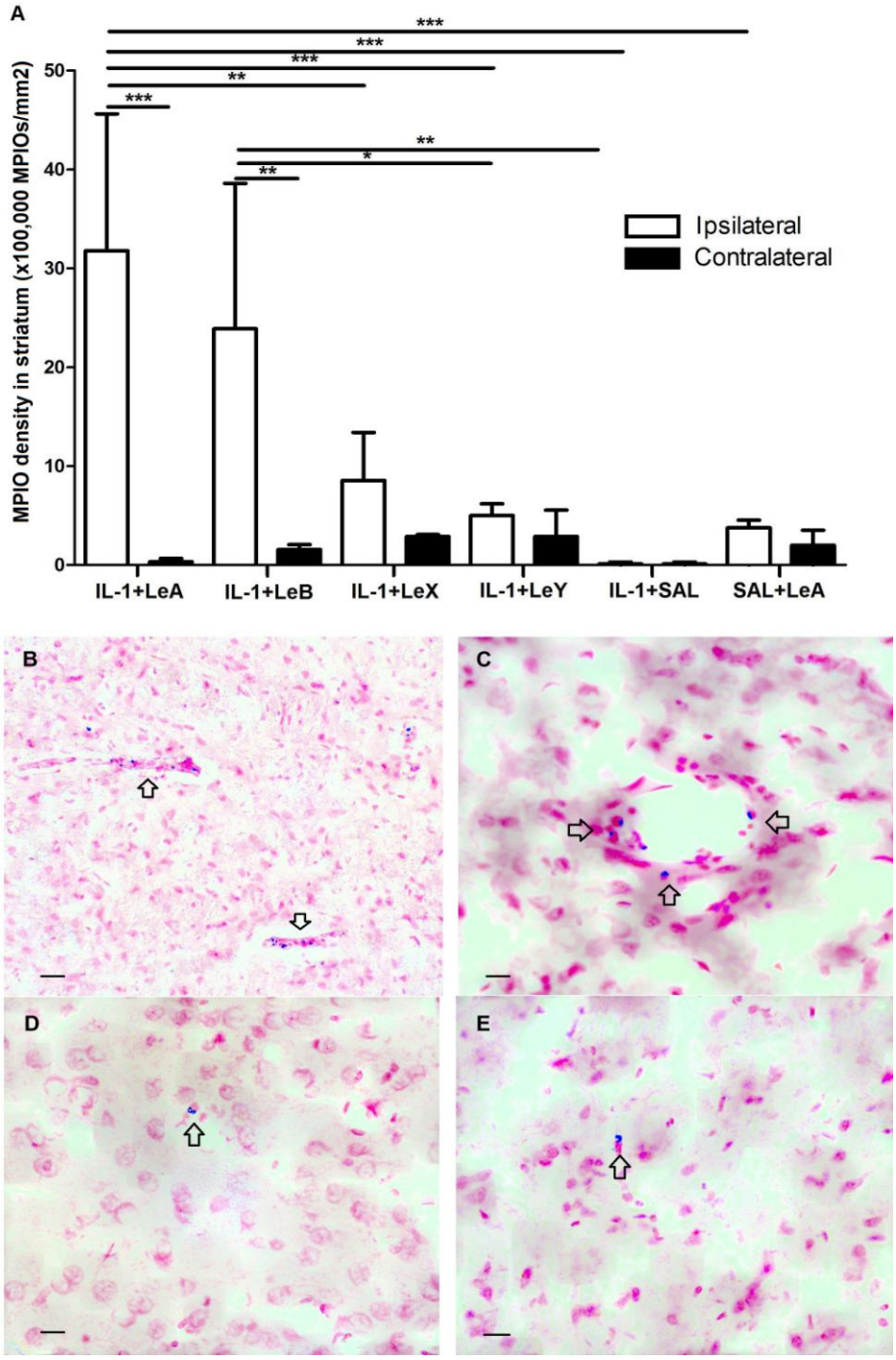

Figure 4. Distribution of Lewis antigen-coated MPIOs in IL-1β-activated rat striatum shown by Prussian blue staining with nuclear fast red. A: Number of MPIOs within the striatum of each of four Lewis sugar-related groups and two control groups. The bars represent the mean ± SEM (n = 3). *P < 0.05; **P < 0.01; ***P < 0.001. SAL, saline. B–E: Distribution of Lewis antigen-coated MPIOs in the ipsilateral striatum of rats injected with Le^A- (B), Le^B- (C), Le^X- (D) or Le^Y- (E) MPIOs. MPIO localizations are indicated by arrows. Scale bars = 200 μm (B) or 100 μm (C–E).

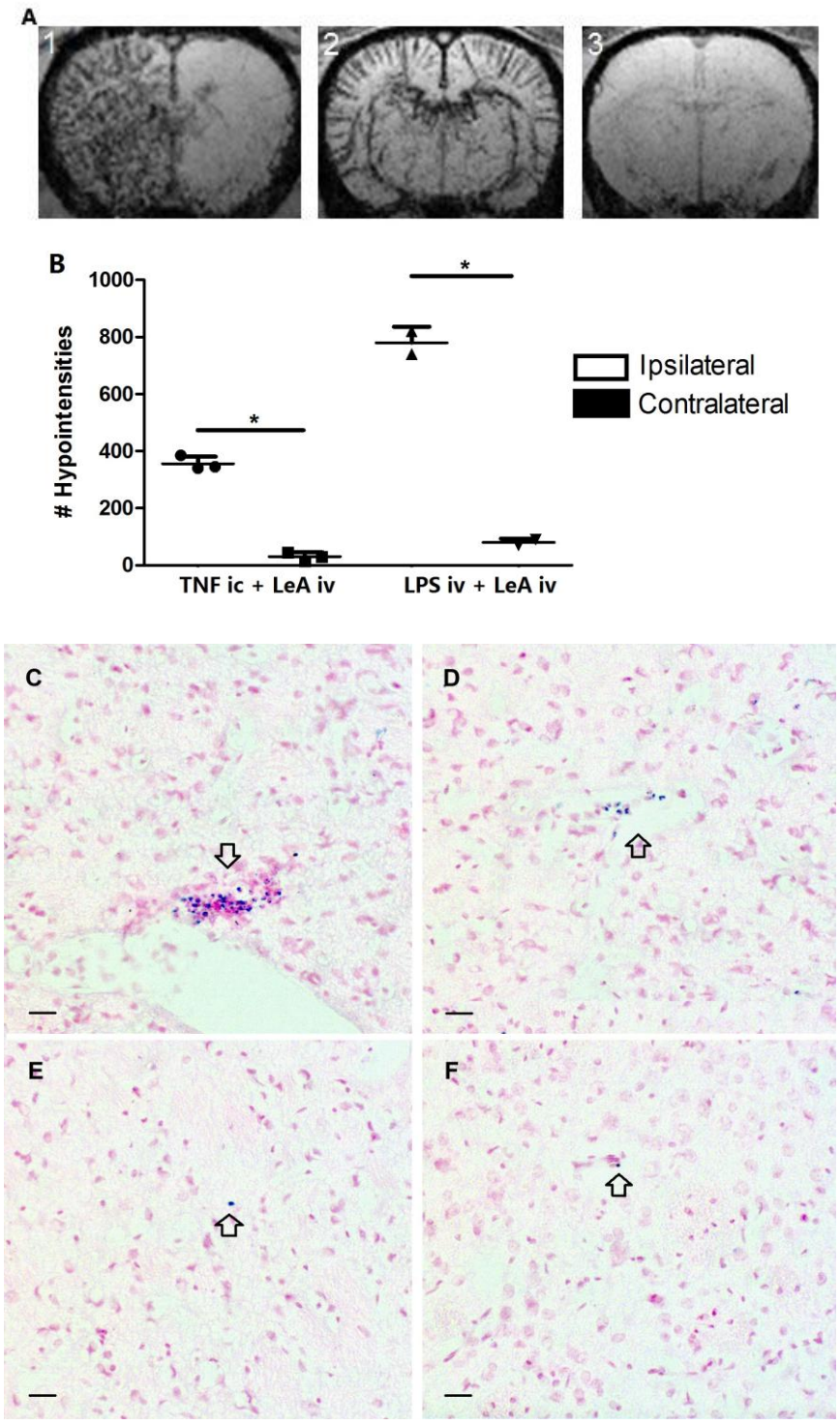

Figure 5. MRI imaging and Prussian blue staining of TNFα- and LPS-activated rat brains to show the distribution of Le^{A}-MPIOs. A: Minimum intensity projections from *in vivo* MRI of Le^{A}-MPIOs after intracerebral injection of TNFα (1), intravenous injection of LPS (2), or intravenous injection of saline (3). *n* = 3 in TNFα ic + Le^{A}-MPIO iv, *n* = 2 in LPS iv + Le^{A}-MPIO iv. All groups and the images shown are representative of the results of all animals in each group. B: Quantification

of the black pixels in the inflamed zone (ipsilateral hemisphere in A1 or both hemispheres in A2) and control zone (contralateral hemisphere in A1 or both hemispheres in A3) from minimum intensity projections after Le^A-MPIO injection. The bars represent the mean ± SEM (n = 2–3). *P < 0.05. ic, intracranial injection; iv, intravenous injection. C–F: Distribution of Le^A-MPIOs, shown by Prussian blue staining with nuclear fast red, in the ipsilateral striatum of rats that had received intracranial TNFα (C–D), intravenous LPS (E), or middle cerebral artery occlusion (as a stroke model) (F). MPIO localizations are indicated by arrows. The staining images shown above are representative of the results of all animals in each group. Scale bars = 100 μm.

Several models have been developed in rodents to simulate the process of acute brain inflammation in neurological disorders (81–82). For example, the pathological changes following middle cerebral artery occlusion (MCAO) in rodents have been reported to be close to those seen in humans with ischaemic stroke, including activation of microvessel walls and a rapid breakdown of the BBB, starting 2 h after occlusion (103). However, in the present study, Prussian blue staining was seldom observed in the rat brain parenchyma after MCAO and Le^A-MPIO injection (Figure 5F). *(Note: The corresponding MRI scanning experiments in the Le^A-MPIO-injected MCAO stroke model are still in progress.)*

Further experiments were performed to determine whether the observed contrast enhancement and aggregated distribution of staining were specifically related to brain inflammation, or whether they could also be observed in control groups. Two control groups were studied: IL-1β-induced brain injury with intravenous injection of saline; and uninjured brain with intravenous injection of Le^A-MPIOs. No significant MRI contrast enhancement was found in either of these control brains (Figure 6A–B). Prussian blue staining revealed only a few blue spots in the uninjured brain, with no obvious, specific patterning (Figure 6D). Similar Prussian blue staining was found in the injured striatum if MPIOs were not injected (Figure 6E). The distribution of charged MPIOs in IL-1β-activated brain parenchyma was

also examined: neither enhancement of intensity projections nor aggregated Prussian blue staining was observed in the ipsilateral striatum after intravenous injection of amine-MPIOs (Figure 6A–C).

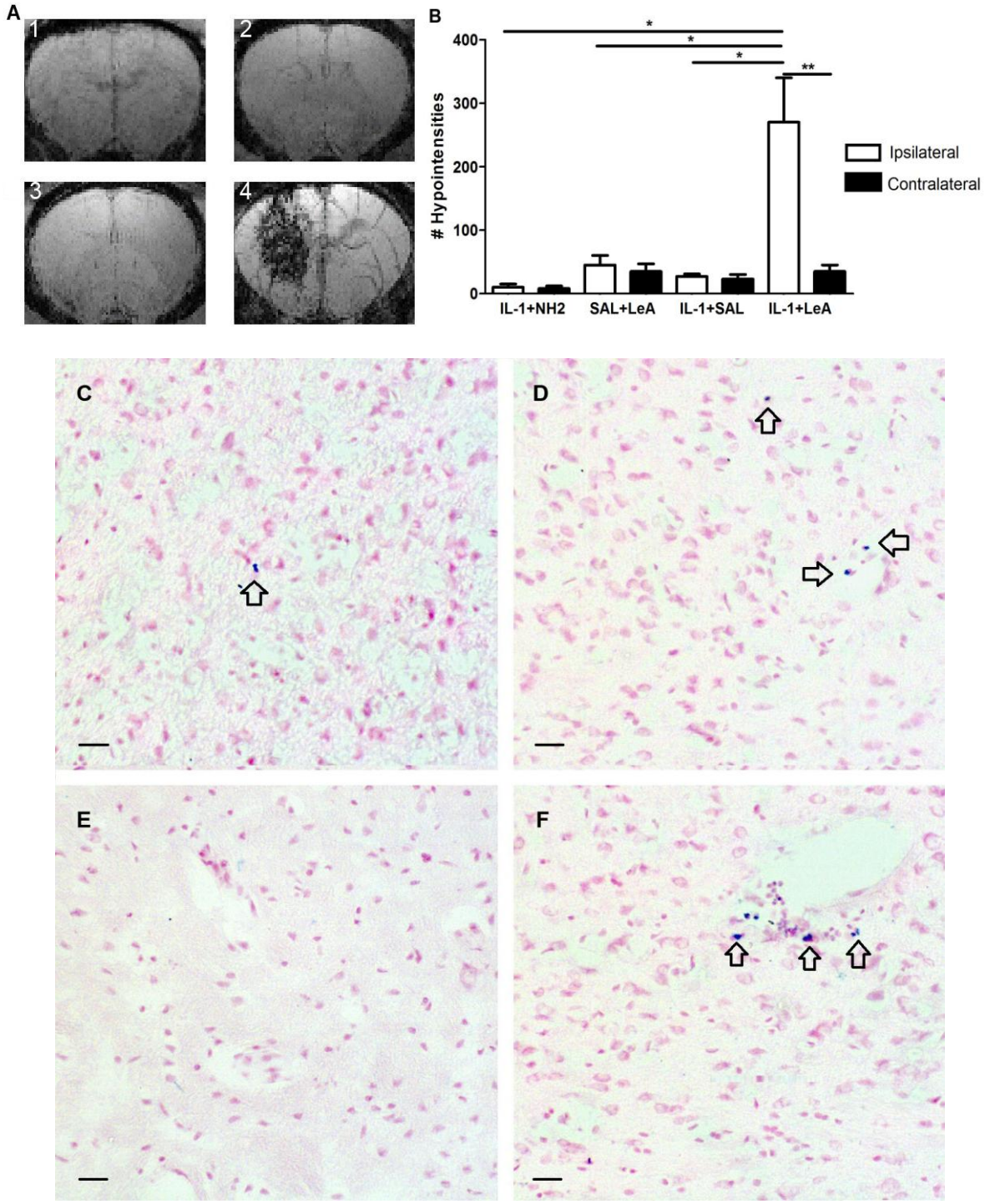

Figure 6. MRI imaging and Prussian blue staining of IL-1β-activated and control brains to show the distributions of Le^{A}-MPIOs and amine-MPIOs. A: Minimum intensity projections from *in vivo*

MRI of rat brains after injections of: (1) IL-1β intracranially (ic) + amine-MPIO intravenously (iv); (2) saline ic + Le^A-MPIO iv; (3) IL-1β ic + saline iv; or (4) IL-1β ic + Le^A-MPIO iv. n = 5 for IL-1β + Le^A, n = 3 for the other groups. Images shown are representative of the results of all animals in each group. B: Quantification of the black pixels in the brain hemispheres from minimum intensity projections. The bars represent the mean ± SEM (n = 5 for IL-1β + Le^A, n = 3 for the other groups). *P < 0.05; **P < 0.01. NH_2, amine-MPIOs. C–F: Distribution of coated MPIOs, shown by Prussian blue staining with nuclear fast red, in the ipsilateral striatum of rats injected with: IL-1β ic + amine-MPIO iv (C); saline ic + Le^A-MPIO iv (D); IL-1β ic + saline iv (E); or IL-1β ic + Le^A-MPIO iv (F). MPIO localizations are indicated by arrows. The staining images shown above are representative of the results of each group. Scale bars = 100 μm.

Effect of Lewis antigen-coated MPIOs on cerebral neutrophil recruitment and BBB integrity

Cerebral neutrophil recruitment is a crucial stage in the exacerbation of CNS inflammation, and is delayed compared with the systemic APR and neutrophil recruitment. Neutrophil infiltration is observed to start from T = 6 h after intracranial injection of IL-1β, with no disruption of the BBB (104). To investigate whether Lewis antigen-coated MPIOs influenced neutrophil migration into the CNS, immunostaining of neutrophils in the ipsilateral striatum (into which IL-1β had been injected) was carried out. There was no detectable neutrophil infiltration into the brain at T = 5 h after intracranial injection of IL-1β (Figure 7B). However, large numbers of neutrophils were observed at T = 5 h when either type of Lewis antigen-coated MPIO was injected intravenously at T = 4 h (Figure 7C–E). The presence of Le^A-MPIOs led to a more substantial elevation of cerebral neutrophil migration than the other Lewis antigen-coated particles (Figure 7A, C–E). Le^A-MPIO injection into uninflamed rat brains was used as a control: there was no detectable enhancement of cerebral neutrophil numbers, at least at T = 5 h (Figure 7A). Moreover, staining of the striatum after amine-MPIO injection also failed to reveal neutrophils at this same time point (Figure 7A).

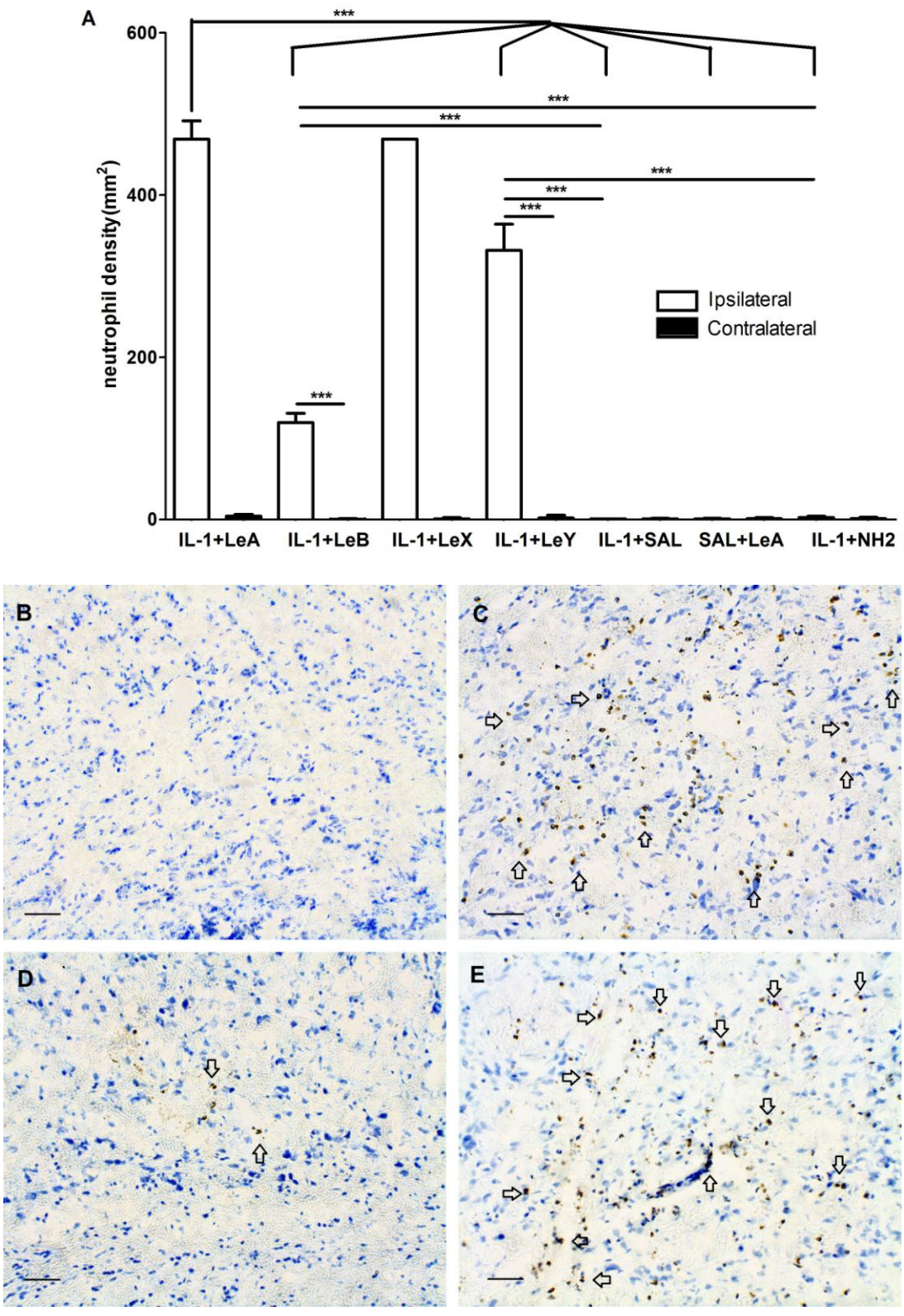

Figure 7. Cerebral neutrophil recruitment in IL-1β-activated brains was enhanced by the intravenous injection of Lewis antigen-coated MPIOs. A: Neutrophil density (cells per mm^2) in the rat striatum of control groups and groups injected with Lewis antigen-coated MPIOs or amine-MPIOs. The bars represent the mean ± SEM (n = 3), except for Le^X-MPIO injection (n = 1). ***P < 0.001. B–

E: Immunostaining of neutrophils, with cresyl violet counter-staining, in the ipsilateral striatum of rats injected with: IL-1β intracranially (ic) + saline intravenously (iv) (B); IL-1β ic + Le^A-MPIOs iv (C); IL-1β ic + Le^B-MPIOs iv (D); or IL-1β ic + Le^Y-MPIOs iv (E). Some neutrophils are indicated by arrows. The staining images shown above are representative of the results of each group. Scale bars = 200 μm.

The enhancement of cerebral neutrophil density may be due to the acceleration of neutrophil infiltration or direct breakdown of the BBB. IgG staining is widely used to measure the permeability of the BBB. Increased BBB permeability allows IgG and other serum proteins to pass into the brain parenchyma where they can be detected by immunostaining. In the present study, the efficiency of IgG staining for the detection of BBB breakdown was demonstrated by the successful staining of MCAO-treated rat brain (Figure 8A). Furthermore, high-intensity IgG staining was observed in the ipsilateral striatum of the Le^A-MPIO-injected group, in contrast to the control group which showed no detectable IgG in the brain parenchyma (Figure 8B–C).

Hepatic and splenic APR after injection of charged MPIOs

As part of the investigation into the pharmacological effects of coated MPIOs, the systemic APR occurring after a dose of coated MPIOs was assessed by measurement of RNA levels using real-time PCR. Time permitted only the potential role of charged MPIOs to be fully investigated in this study. These experiments were conducted using IL-1β-injured mouse brains, which show a similar contrast enhancement of the hemispheres to rat brains after the injection of Le^A-MPIO, with less hypointensities in mice when injecting Le^B-MPIOs (Figure 9). To maximize the potential effect of charged MPIOs on the APR, MPIOs (intravenously) and IL-1β (intracranially) were injected together at T = 0 h, and left for 4 h

before their effects were determined. GAPDH was selected as the reference gene for determining the relative expression of APPs using real-time PCR.

There exist two methods to quantify the results obtained by real-time PCR with similar approach these days. One is called comparative Ct method (ΔCt method), in which the Ct values of the samples of interest are compared with that of a non-treated sample from normal tissue. The Ct values of both the samples of interest and the non-treated sample are normalized to an appropriate endogenous housekeeping gene before the comparison, which is also known as 2-ΔΔCt method. Here, ΔΔCt = ΔCt sample – ΔCt reference, where ΔCt sample is the Ct value of samples normalized to housekeeping gene, and ΔCt reference is the Ct value of calibrators normalized. The premise of using such method is that the amplification efficiencies of the target and the reference genes should be approximately equal.

In this project, there are many target genes in APR study and it is infeasible to choose a housekeeping gene with similar efficiency to all interests. Therefore, another method using standard curve is applied. Firstly, a series of template solutions with known RNA concentration is used to construct standard curves of each gene. These curves are then for extrapolating quantitative information for mRNA targets of unknown concentrations. The advantage of this method is that replicating efficiencies of different genes can be represented by the gradient of standard curves. For example, if the standard curve has a gradient of larger than 3.3 in its absolute value, the related replicate efficiency will then be lower than 95% and should be discarded from analysis. Before our testing on APR-related genes, control RNA expression of GAPDH had been found stable in various tissues of all groups comparing with the expression of other housekeeping genes such as β-actin (data not shown). The results of real-time PCR indicated that the expression of selected pro-inflammatory mediators, including IL-6, TNFα, chemokine (C-C motif) ligand 2 (CCL2), chemokine (C-X-C motif) ligand 1 (CXCL1), and CXCL10, was inhibited by amine-MPIOs but not carboxylic-MPIOs

(Figure 10, 11). TNFα and CCL2 were downregulated by 40–80% in the liver (Figure 10C, F) and spleen (Figure 11C, F), compared with IL-1β-activated mice not receiving MPIO injection. Other effects of amine-MPIOs on pro-inflammatory mediators included a 70% suppression of hepatic IL-6 levels (Figure 10B) and a 40% suppression of splenic CXCL10 levels (Figure 11E). In contrast, the injection of charged MPIOs was not associated with any peripheral changes in IL-1β (Figure 10A, 11A) or CXCL1 (Figure 10D, 11D) expression levels.

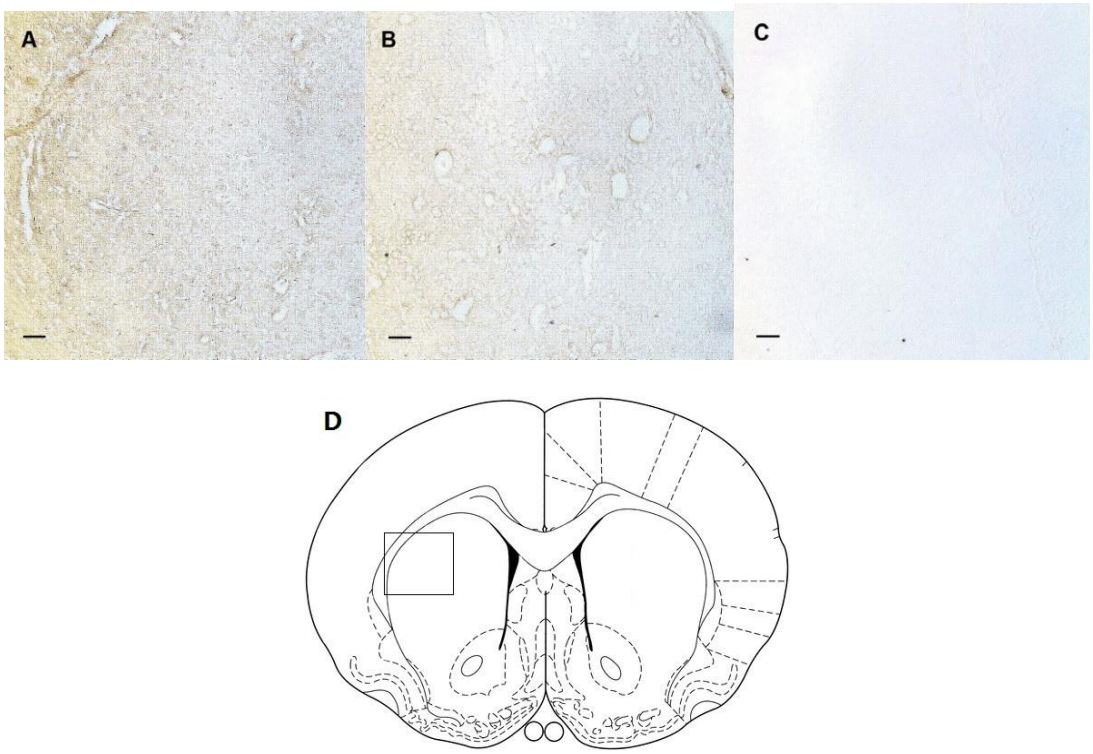

Figure 8. BBB disruption mediated by Le^A-MPIOs in IL-1β-injured rat brain shown by IgG staining. A–C: IgG staining of the ipsilateral striatum in rats treated with: 2h of middle cerebral artery occlusion (MCAO) and 4h of reperfusion (A); IL-1β intracranially (ic) + Le^A-MPIO intravenously (iv) (B); or saline ic + Le^A-MPIO iv (C). The rat brain after MCAO treatment is as the positive control, and the saline-injected group is as the negative control. Scale bars = 500 μm. (D) The rectangle indicates the approximate area of the rat brain corresponding to the IgG-stained images shown in A–C, according to the atlas of Paxinos and Watson (105).

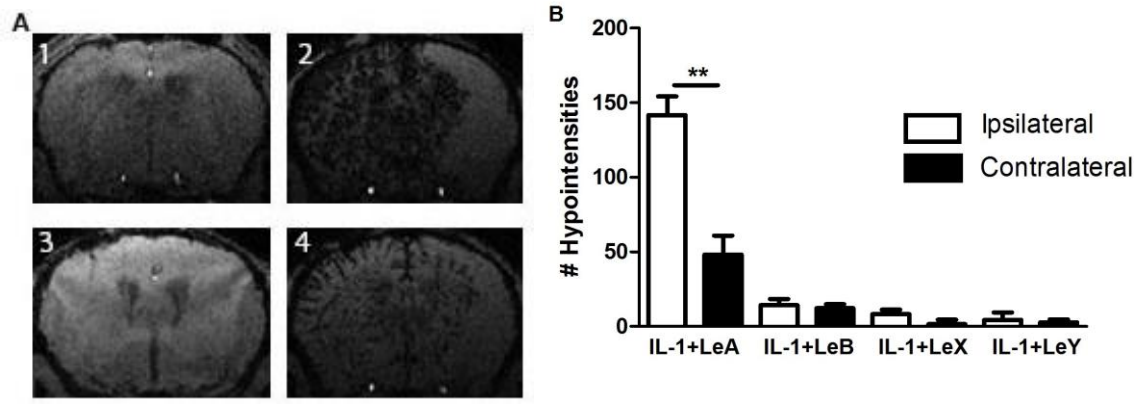

Figure 9. MRI contrast enhancement in the IL-1β-injured mouse brain after intravenous injection of Le^{A}-MPIOs. A: Minimum intensity projections from *in vivo* MRI of the left hemispheres of the brains of mice injected with IL-1β and: Le^{X} (1); Le^{A} (2); Le^{Y} (3); or Le^{B} (4). B: Quantification of the black pixels in minimum intensity projections of the ipsilateral (IL-1β) and contralateral (control) brain hemispheres after injection of four types of Le-MPIOs respectively. The bars represent the mean ± SEM (n = 3). $^{**}P < 0.01$; $^{***}P < 0.001$.

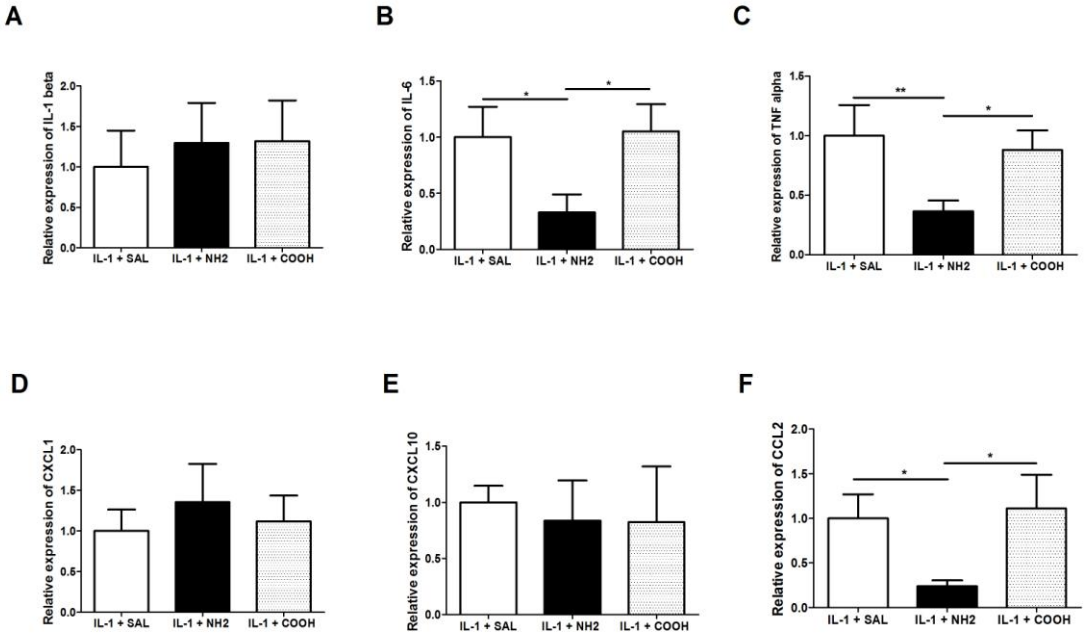

Figure 10. Effects of charged MPIOs on hepatic expression of pro-inflammatory mediators in IL-1β-injured mice (T = 4 h). The relative expressions (GAPDH as the reference gene) of IL-1β (A),

IL-6 (B), TNFα (C), CXCL1 (D), CXCL10 (E) and CCL2 (F) were normalized to the IL-1β + SAL group. COOH, carboxylic-MPIOs. Bars represent the mean ± SEM (n = 3–4). *P < 0.05; **P < 0.01.

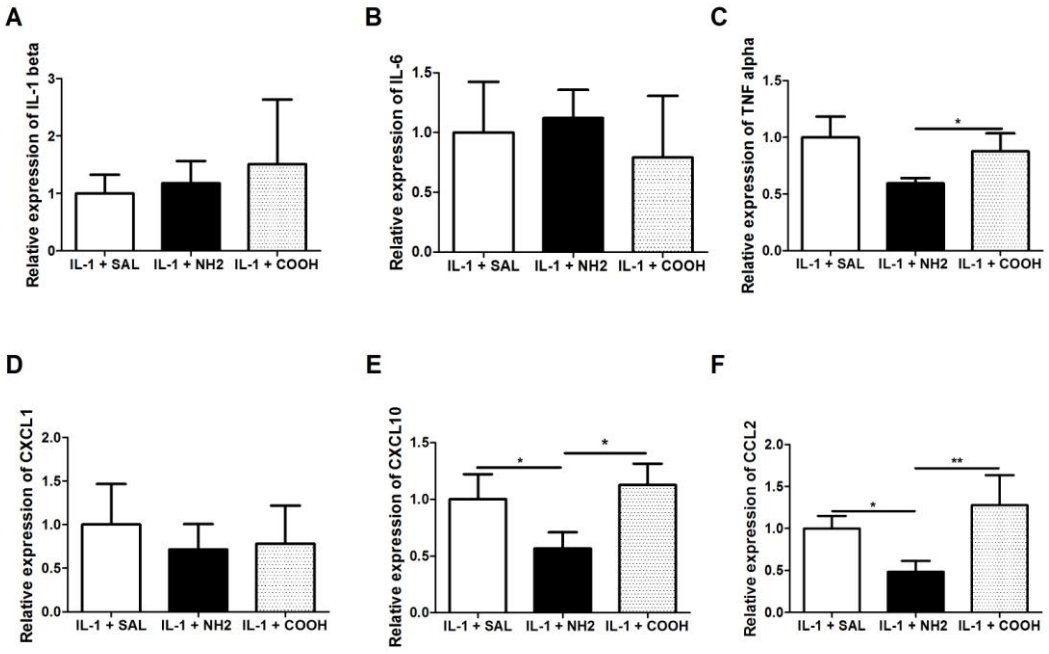

Figure 11. Effects of charged MPIOs on the splenic expression of pro-inflammatory mediators in IL-1β-injured mice (T = 4 h). The relative expressions (GAPDH as the reference gene) of IL-1β (A), IL-6 (B), TNFα (C), CXCL1 (D), CXCL10 (E) and CCL2 (F) were normalized to the IL-1β + SAL group. COOH, carboxylic-MPIOs. The bars represent the mean ± SEM (n = 3–4). *P < 0.05; **P < 0.01.

The hepatic and splenic expression of anti-inflammatory cytokines, after acute brain injury and MPIO injection, was investigated using measurements of the RNA levels of IL-4, IL-10 and transforming growth factor-β (TGF-β). No regulatory effect of charged MPIOs on the expression of these anti-inflammatory cytokines was detected (Figure 12). The expression levels of other subtypes of APPs, such as adhesion molecules and cyclooxygenases (COXs), were also measured. E-selectin was shown to be downregulated (or there was an apparent trend towards downregulation) in the liver and spleen by both amine-MPIOs and carboxylic-MPIOs (Figure 13A–B), while the VCAM-1 level was consistent irrespective of the organ

tested and the charge on the particles (Figure 13C–D). Amine-MPIOs were found to suppress the hepatic expression of COX-1, while carboxylic-MPIOs elevated hepatic COX-2 expression without affecting COX-1 levels (Figure 14). In general, most of the APPs assessed were regulated by amine-MPIOs but not carboxylic-MPIOs.

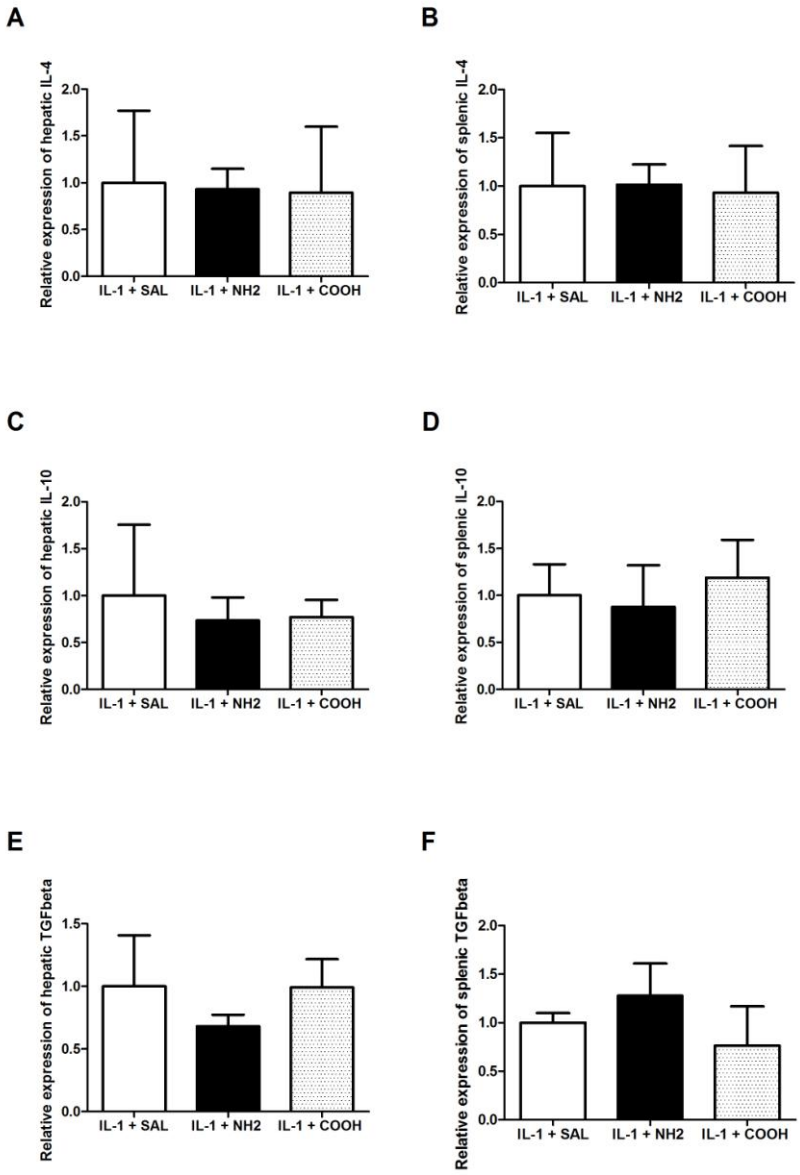

Figure 12. Effects of charged MPIOs on the peripheral expression of anti-inflammatory mediators (T = 4 h) in mice injected intracranially with IL-1β. The relative expressions (GAPDH as the reference gene) of IL-4 (A–B), IL-10 (C–D) and TGF-β (E–F) in the liver and spleen were normalized to the IL-1β + SAL group. SAL, saline. The bars represent the mean ± SEM (*n* = 3–4).

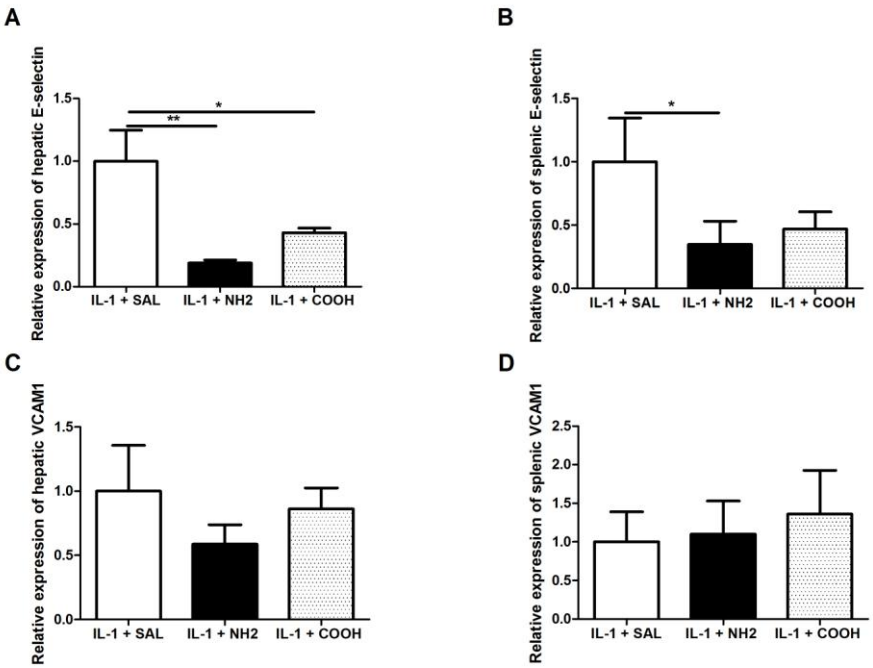

Figure 13. Effects of charged MPIOs on the peripheral expression of adhesion molecules (T = 4 h) in mice injected intracranially with IL-1β. The relative expressions (GAPDH as the reference gene) of E-selectin (A–B) and VCAM-1 (C–D) in the liver and spleen were normalized to the IL-1β + SAL group. SAL, saline. The bars represent the mean ± SEM (n = 3–4). *P < 0.05; **P < 0.01.

Effect of charged MPIOs on systemic neutrophil recruitment, BBB integrity and GLUT1 expression

Acute brain injury triggers hepatic chemokine release and leukocyte recruitment to the liver that starts at T = 2 h (26), and cerebral leukocyte recruitment that occurs after T = 6 h (106). In this study, intracranial injection of IL-1β was capable of inducing neutrophil recruitment to the liver, but not the brain or spleen, at T = 4 h (Figure 15). It is hypothesized that hepatic neutrophil migration may be suppressed by amine-MPIOs as a consequence of the observed APR downregulation. At T = 4 h after IL-1β injection, hepatic neutrophil recruitment was suppressed by the injection of amine-MPIOs but not carboxylic-MPIOs (Figure 15A). No modulation of splenic or cerebral neutrophil migration was observed at T = 4 h after the injection of charged MPIOs into mice injected with IL-1β (Figure 15B–C).

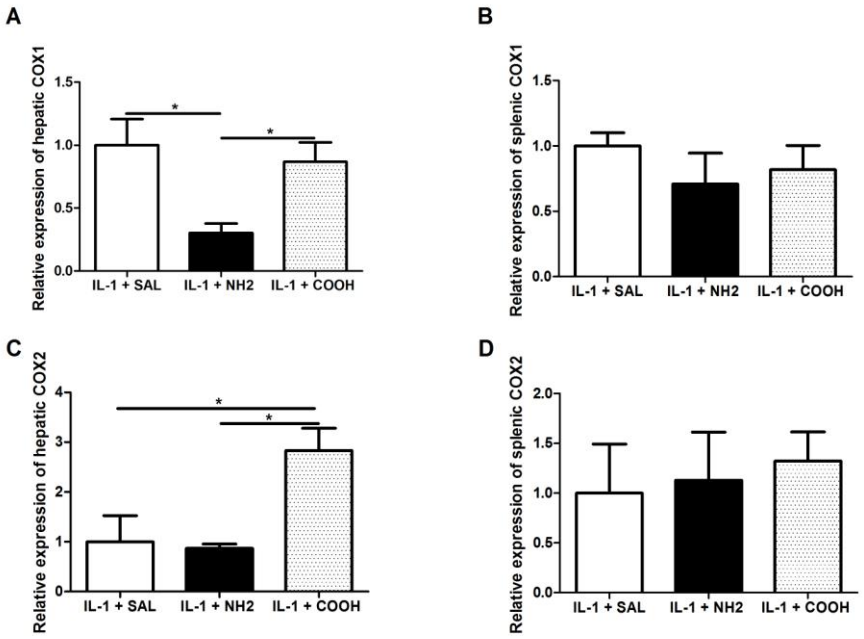

Figure 14. Effects of charged MPIOs on the peripheral expression of COXs (T = 4 h) in mice injected intracranially with IL-1β The relative expressions (GAPDH as the reference gene) of COX-1 (A–B) and COX-2 (C–D) in the liver and spleen were normalized to the IL-1β + SAL group. SAL, saline. The bars represent the mean ± SEM (n = 3–4). *P < 0.05.

With regard to the BBB, no IgG staining was found in the IL-1β-injured ipsilateral striatum after injection of amine-MPIOs or saline (Figure 16A, D). The expression of glucose transporter protein 1 (GLUT1), a uniporter protein on the BBB, was also visualized by immunostaining. A downregulation of GLUT1 levels on the plasma membrane of brain endothelial cells has been reported to be associated with BBB dysfunction and leukocyte infiltration (107). Furthermore, GLUT1, which is regarded as an APP, is upregulated by IL-1β and is also essential for glycan production on cell surfaces (108). From the staining results obtained in the present study, it was clear that GLUT1 expression in brain parenchyma was induced by IL-1β intracranial injection (Figure 16C, F), but was not modulated by amine-MPIOs (Figure 16B).

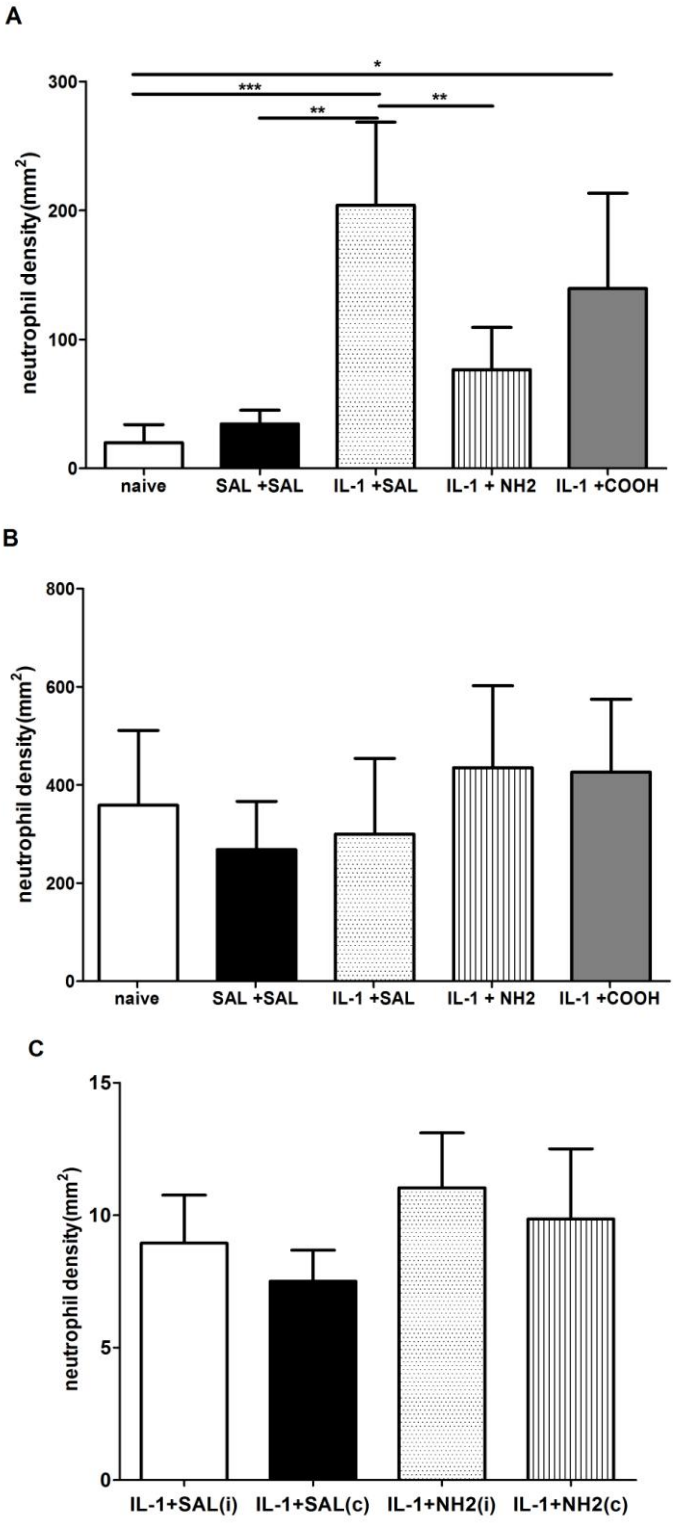

Figure 15. Systemic neutrophil recruitment after intravenous injection of charged MPIOs. Hepatic (A), splenic (B) and cerebral (C) neutrophil density (cells per mm^2) at T = 4 h after IL-1β and MPIO injection. Only slices injected with amine-coated MPIOs were counted. i, ipsilateral; c,

contralateral. The bars represent the mean ± SEM (n = 3–4 for A and B, n = 2 for C). *P < 0.05; **P < 0.01; ***P < 0.001.

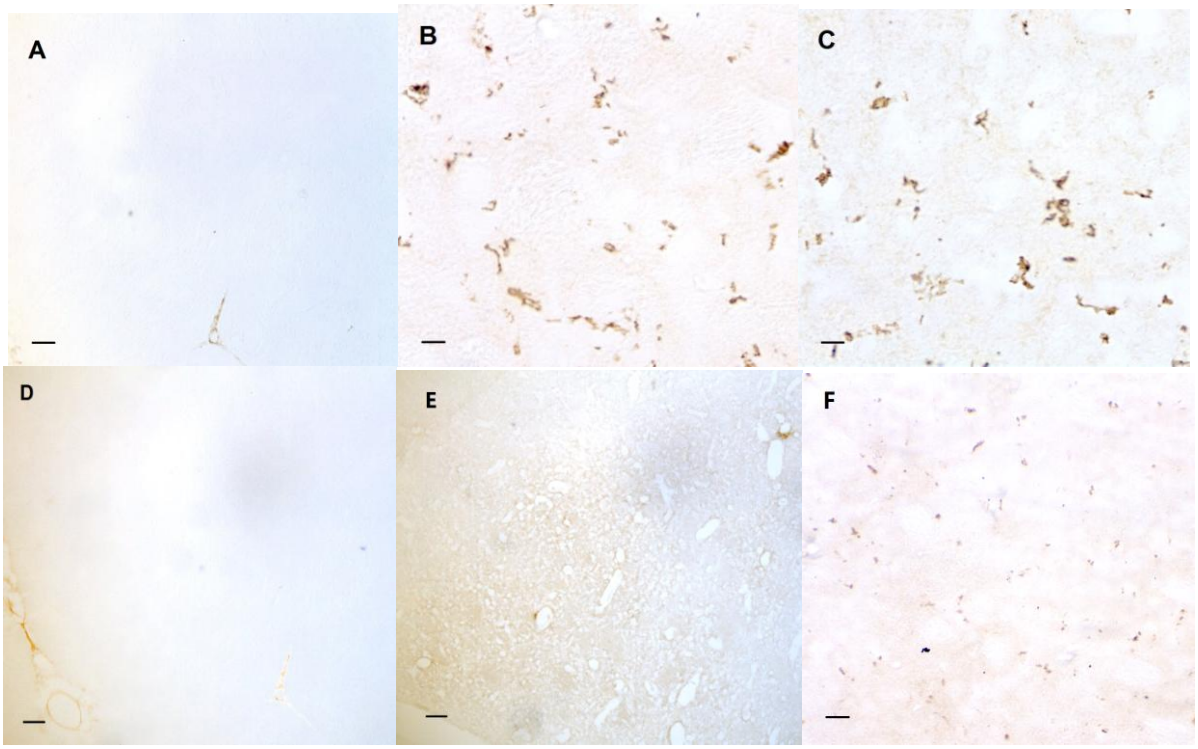

Figure 16. IgG and GLUT1 immunostaining of mouse brain after amine-MPIO injection. A, D, E): IgG staining of the ipsilateral striatum at T = 4 h after IL-1β ic + amine-MPIO iv injection (A), or after IL-1β ic + saline iv injection (D), or after MCAO treatment (E). Scale bars = 500 μm. B, C, F): GLUT1 staining of the ipsilateral striatum at T = 4 h after IL-1β ic + amine-MPIO iv injection (B), or after IL-1β ic + saline iv injection (C), or after saline ic + saline iv injection (F). Scale bars = 100 μm.

Effect of amine-MPIOs on systemic cytokine/chemokine expression and residential leukocyte density in uninflamed tissue

Cytokines and chemokines have a low level of constitutive expression in healthy individuals (109). To investigate whether this constitutive expression of cytokines/chemokines is regulated by amine-MPIOs, amine-MPIOs were injected into healthy mice, and the expression levels of specific APPs found to have been suppressed by

amine-MPIOs in IL-1β-injured mice were measured. All these APPs maintained a consistent level of expression in healthy mice irrespective of amine-MPIO injection (Figure 17A–F).

The systemic neutrophil density is another physiological parameter depicting the early process of inflammation. Unlike the suppression observed in IL-1β-injured mice, amine-MPIOs did not elicit changes in the neutrophil densities of liver, spleen or brain parenchyma of healthy mice at T = 4 h after injection (Figure 17G–H). The density of activated microglia in the brains of healthy mice was also not affected by amine-MPIOs *in vivo* (Figure 17I).

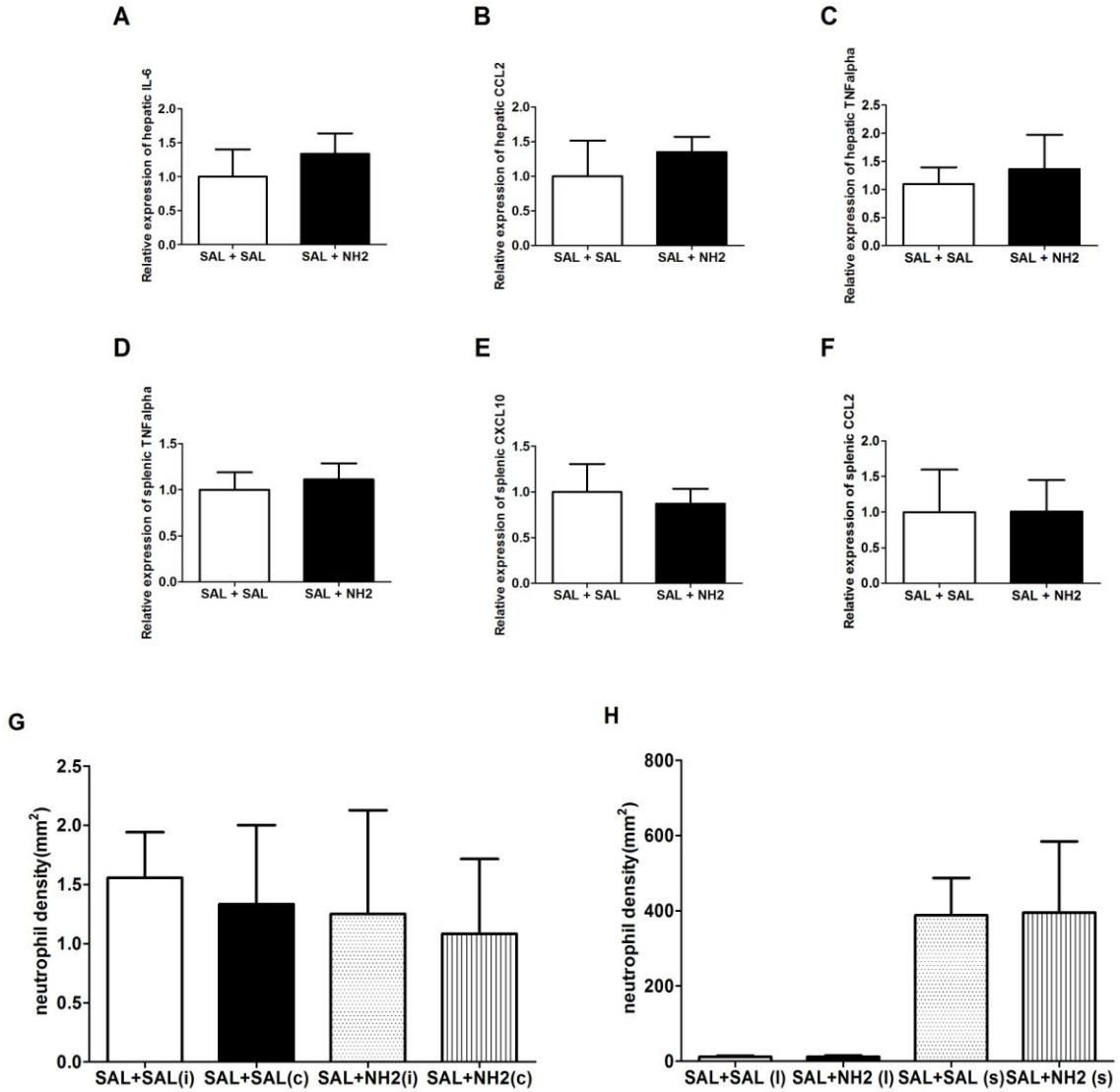

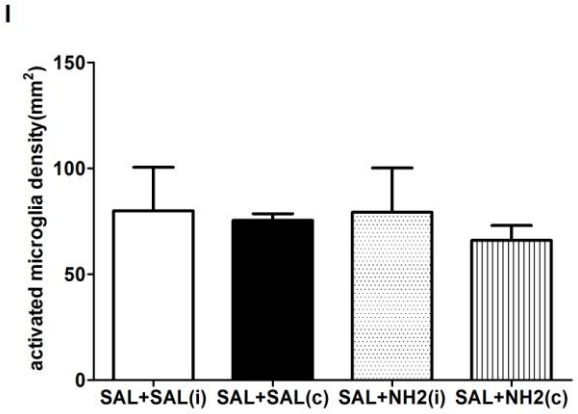

Figure 17. Systemic APP expression and residential leukocyte density in healthy mice after amine-MPIO injection. A–F: Effects of amine-MPIOs on the residential expression of pro-inflammatory mediators in the livers (A–C) and spleens (D–F) of healthy mice. GAPDH was used as the reference gene, and normalisation was undertaken. All the APPs studied in these experiments were suppressed by amine-MPIOs in IL-1β-injured mice. The bars represent the mean ± SEM (*n* = 3–4). G–H: Effect of amine-MPIOs on the residential density of cerebral neutrophils (G), peripheral neutrophils (H) and cerebral activated microglia (I) in healthy mice. The bars represent the mean ± SEM (*n* = 3–4). "i" – ipsilateral, "c" – contralateral, "l" – liver, "s" – spleen.

Discussion

Taken together, the results from the immunostaining and Prussian blue staining experiments indicate that, during acute brain inflammation induced by IL-1β, only Le^A/Le^B-MPIOs show overlap with structures similar to activated endothelium in the brain parenchyma. In addition, Le^A-MPIOs were also observed to potentially co-localize with brain microvessels or other structures after intracranial injection of TNFα, suggesting that there may be Le^A-targeted molecules, currently of unknown identity, along the activated blood vessels that are upregulated by stimulation with either IL-1β or TNFα. All the staining results were in accordance with the MRI data, revealing an ability of Le^A to enhance the contrast through specific binding. No Prussian blue staining was observed along the blood vessels in the striatum after intravenous injection of LPS; this is similar to the MRI results, which

showed intensity projections mainly along the cortical vessels or the lateral ventricle. The lack of Prussian blue staining of the ipsilateral hemisphere in the MCAO stroke model may have been due to severe disruption of endothelial structures, since IgG staining in the MCAO model suggested that the BBB had largely been broken down. In conclusion, Le^A-MPIOs have been demonstrated to permit the effective imaging of inflamed sites in the CNS through binding to endothelial cell-like structures. Moreover, the results of the Prussian blue staining closely paralleled the MRI intensity patterns.

IL-1β or TNFα-mediated acute brain injury has been shown not to affect the integrity of the BBB (104). Although Le^A/Le^B-MPIOs appear to bind to activated endothelium in the brain parenchyma, it was not previously known whether these glycan-coated particles would also enhance the MRI contrast when the endothelium of the BBB is disrupted. During my research, I was not able to observe any specific distribution of Prussian blue staining in the brain either after systemic injection of LPS infection or in the MCAO-treated rat model. It is well known that systemic injection of LPS can impair BBB integrity (110), induce cytokine release by brain endothelial cells (111), and alter the transporting systems on the BBB (112). In addition, MCAO also leads to a rapid breakdown of the BBB within hours (103). Therefore, it is likely that these glycan-coated MPIOs are not able efficiently to depict inflamed sites during BBB breakdown. This could be tested by applying Le^A/Le^B-MPIOs for MRI during the later stages of ischaemic stroke, or for MRI of chronic brain injuries mediated by adenoviral overexpression of cytokines.

The effect of type I Lewis antigen on the MRI contrast enhancement is slightly different when comparing mice and rat results. Specifically, Le^B-MPIOs accumulated in the inflamed sites of the rat but not mice ipsilateral hemisphere, suggesting that the expressional pattern of some surface molecules on BBB might be different. Although the BBB permeability is similar in mice and rats (113), the distribution of receptors, enzymes, and

transporters including P-glycoprotein are known to have species differences (114). The primary approach for the reason of less hypointensities in mice brain could be analyzing the expression of some potential receptors of Lewis residues.

The acceleration of cerebral neutrophil recruitment is a novel pharmacological role of Lewis antigen-coated MPIOs. Although these MPIOs were injected only 60 minutes before terminal anaesthesia, neutrophils were observed rapidly to infiltrate brain parenchyma in large numbers. Normally, neutrophils only start to appear 6 h after intracranial injection of IL-1β (104). The early presence of neutrophils in the striatum at T = 5 h may have been due to BBB disruption, as implied by the results of IgG staining experiments (albeit with low replicability: only 2 of the 5 brains in the Le^A-MPIO-injected group showed evidence of IgG staining), or elevation of the systemic inflammatory response; these possibilities require further investigation. There are several alternative methods to IgG staining as a means to assess the integrity of the BBB, including immunostaining of tight junction proteins such as ZO-1, occludin-1 and claudin-5. Other possible techniques include staining with horseradish peroxidase (HRP), which can penetrate the disrupted BBB by perfusion, or Evans blue staining to detect albumin in the brain parenchyma (115). Experiments such as these will enable a more definitive conclusion to be drawn as to whether the BBB permeability is substantially elevated by unsialylated Lewis residues.

In addition to causing BBB breakdown, Lewis antigen-coated MPIOs may also disrupt normal BBB functions by mimicking the characteristics of leukocytes *in vivo*. These MPIOs may have the potential to be recognized as leukocytes by the BBB due to the hypothesized opsonisation happens on their surface. Circulating leukocytes normally extravasate across the vascular wall of the activated endothelium, leading to the accumulation of leukocytes in the perivascular space of the CNS. This transmigration step can occur through paracellular pathways between adjacent endothelial cells, or via trans-endothelial

migration directly through the endothelial cell itself, leaving inter-endothelial cell junctions intact (116–117). Considering the specific distribution of Le^A/Le^B-MPIOs along activated endothelium, it is possible that these particles may also affect the leukocyte transmigration pathway in addition to BBB integrity. Certain adhesion molecules have been identified as key mediators of leukocyte extravasation; many of these, such as CD31, CD99 and ICAMs, are expressed at the luminal endothelial surface as well as at tight junctions, and can contribute to both paracellular and trans-endothelial pathways. Other adhesion molecules, including the junctional adhesion molecules (JAMs) and VE-cadherin, are expressed exclusively at endothelial cell junctions and may contribute solely to the paracellular pathway (118–120). The expression levels of these molecules following the injection of glycan-coated particles remain to be determined by immunostaining and ELISA.

The endothelial release of pro-inflammatory cytokines and chemokines during inflammation has received much attention in recent years. An upregulation of these APPs by Lewis antigen-coated MPIOs would provide an additional explanation for the observed acceleration of cerebral neutrophil recruitment. Several chemokines have been found to be selectively upregulated by injured microvascular endothelium. These chemokines include CXCL8, CXCL10 and CCL2 in response to inflammatory cues such as TNFα, histamine and thrombin (121–123). A number of chemokines have also been identified in *in vitro* cultures of brain activated microvascular endothelial cells, such as CCL2, CCL4 and CCL5 (124–125). These molecules bind to chemokine receptors expressed by activated mononuclear cells, including CCR1, CCR2 and CCR5 (126). Further research is necessary, utilizing *in vitro* as well as *in vivo* approaches, to elucidate the potential effects of Lewis antigen-coated MPIOs on the endothelial expression of chemokines, and to identify any additional mechanisms, other than the hypothesized BBB disruption or the possible acceleration of leukocyte transmigration, underlying enhanced cerebral neutrophil recruitment.

Identification of the ligand(s) for Le^A/Le^B-MPIOs on IL-1β-activated endothelium will help to delineate the mechanisms by which Lewis glycans adhere to the BBB and potentially affect its function. In the search for such a ligand, DC-SIGN and its homolog, DC-SIGNR, merit careful investigation, as they are known to recognise all four Lewis antigens. Both DC-SIGN and DC-SIGNR have been of considerable interest in immunological research because of their ability to bind to human immunodeficiency virus and present exoligands to T lymphocyte cells, which greatly facilitates the efficacy of infection (127). DC-SIGN binds strongly to the fucose structures in all four Lewis residues during the capture of LPS or other exogenous ligands (128), implying that intravenously injected Le^A-MPIOs and LPS may compete for binding to DC-SIGN. Such a hypothesis might explain the paucity of aggregated Prussian blue dots in the ipsilateral striatum after intravenous injection of LPS (Figure 5). Moreover, DC-SIGN and DC-SIGNR can also bind to endogenous ligands. For instance, DC-SIGN mediates the adhesion of dendritic cells to activated endothelium by binding to Le^Y expressed on ICAM-2 (129). DC-SIGN also leads to the transient adhesion of dendritic cells with T cells through binding to Le^X on ICAM-3, supporting the stabilization of immunological synapses and T-cell priming (130). The similar ligand affinities of DC-SIGN and DC-SIGNR are due to their CRD domains, which are tetramerized for carbohydrate recognition; polymorphisms in the CRD motif may determine the slight differences in adhesion to certain Lewis antigen subtypes (131). It is possible that some subtypes of DC-SIGN or DC-SIGNR may have greater affinity for Le^A than for other Lewis glycans.

DC-SIGNR has very different patterns of expression to DC-SIGN. DC-SIGN is highly expressed in monocytes and monocyte-derived dendritic cells in tissues such as spleen and lung. In contrast, the expression of DC-SIGNR is limited to the endothelial cells in lymph nodes, liver and intestinal tissues (131); to date, there have been no reports regarding its potential distribution along the BBB. Screening of mouse cDNA libraries has led to the

identification of 8 mouse homologues of DC-SIGNR, designated SIGNR1 to SIGNR8 (132). Glycan-array screening of these mouse homologues has shown that only mouse SIGNR3 shares the ability of human DC-SIGN to bind both fucose- and mannose-terminated glycans for endocytosis, raising the possibility that SIGNR3 may be one of the endothelial ligands for Le^A-MPIOs. Preliminary results from our laboratory using SIGNR3 knockout (KO) mice have supported this possibility, since a statistically significant difference in Le^A-MPIO binding was observed between wild-type (WT) and SIGNR3 KO mice (Figure 18; $P < 0.01$, Student's *t*-test). This finding also provides, for the first time, indirect evidence for the existence of SIGNR3 along brain endothelial cells. However, binding of the particles was not completely suppressed in SIGNR3 KO mice, suggesting that other receptors may also be responsible for particle binding. Such additional receptors may include SIGNR5 (which shows preferential binding of mannose over fucose), SIGNR2 (which binds exclusively to glycans bearing terminal GlcNAc residues), SIGNR5 (which shows preferential binding to 6-sulfo-sLe^X), or cell adhesion molecules such as selectins, VCAM-1, ICAM-1 and CD31. Identifying the molecular targets could be achieved using MRI in mice with gene deletions, Le^A-MPIO pull-down assays, or ELISA in magnetic fields.

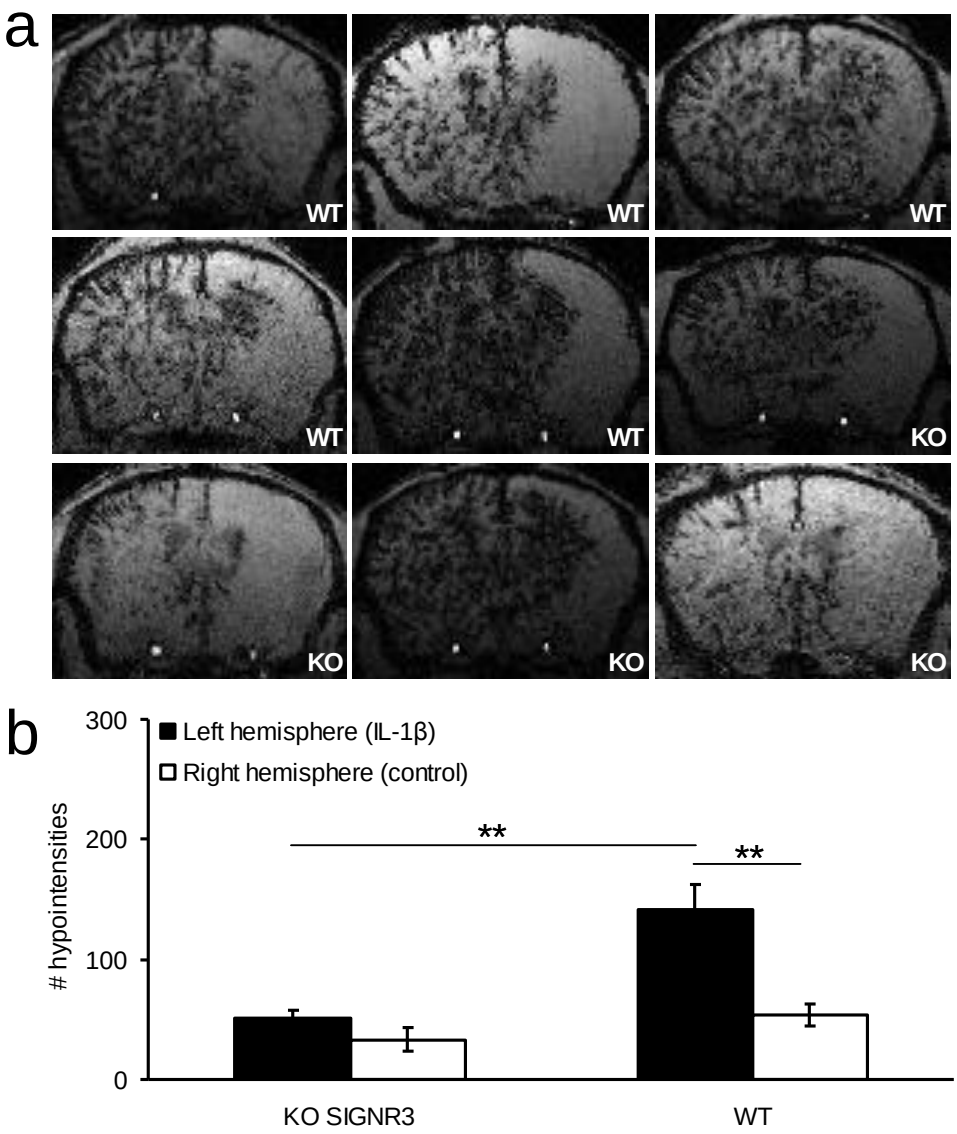

Figure 18. MRI of IL-1β-injured SIGNR3 KO mice injected with Le^A-MPIOs. A: Minimum intensity projections from *in vivo* MRI of the brain in WT and SIGNR3 KO mice after intracerebral injection of IL-1β into the left hemisphere and intravenous injection of Le^A-MPIOs. n = 5 for WT mice and n = 4 for SIGNR3 KO mice. The images shown are the list of all mouse brain results. B: Quantification of the black pixels in the minimum intensity projections of the left (IL-1β) and right (control) brain hemispheres. The bars represent the mean ± SEM. **$P < 0.01$. (left hemisphere of WT versus KO; and left versus right hemisphere in WT). Authorized by Guillaume Bort.

Certain issues need to be addressed before further use of these Le^A/Le^B-MPIOs in clinical applications, in addition to determination of the molecular ligands and the potential

effect on BBB integrity. First, the circulation time of Le^A/Le^B-MPIOs in the blood and their potential toxicity should be investigated, as mentioned later in this discussion. Second, although it is clear from Prussian blue staining that the glycan-coated MPIOs are co-localized on activated endothelium, it remains unknown whether these MPIOs adhere only to endothelial cells, or whether they are also carried by leukocytes arrested on the endothelial cells. Counterstaining of slices and fluorescence imaging of particles in cultured cells should be carried out to investigate this issue. Third, as Le^A/Le^B-MPIOs may bind to DC-SIGN or DC-SIGNR along cerebral vessels or in lymphoid tissues, these glycan-coated particles are theoretically capable of modulating systemic inflammatory responses during CNS inflammation. Therefore, the hepatic and splenic APR after Le^A-MPIO injection should be assessed by real-time PCR and immunostaining, as was done in the present study for the injection of charged MPIO. Fourth, a comprehensive study of how the surface charges of MPIOs affect systemic inflammation is essential to determine the best way to optimize the pharmacological effects of existing glycan-coated particles by the addition of charges.

A systemic effect of charged particles on the APR and neutrophil recruitment *in vivo* has not been reported previously. Other *in vitro* studies have revealed that amine-MPIOs can induce cytokine release, apoptosis and endocytosis in cultured macrophages and fibroblasts, as markers of the cytotoxicity of these particles (41). However, these phenomena only existed from T = 24 h after MPIO incubation, a very different time point to the one tested in the present study (T = 4 h). In addition, it should be noted that *in vitro* binding data may not be replicated well in complicated *in vivo* systems (133) due to competitive binding with other charged proteins, the local concentration of ligands, and the hydrodynamics in the circulation. Many studies have investigated protein adsorption onto polymeric particles with distinct surface properties (134–135), and the relationship between the chemical composition of particles and their *in vivo* distribution (136). Furthermore, although many cell types

(neutrophils, mast cells, macrophages, etc.) have been well documented to release cytokines after endocytosis, macrophages are more frequently found to engulf biomaterial particles with different surface characteristics (137), and are the only cell type that are induced to undergo apoptosis, rather than necrosis, by standard polystyrene beads (138). With regard to cytokine release, macrophages exposed to polymethylmethacrylate, cobalt chromium molybdenum alloy, titanium alloy, polyethylene or polyurethane particles all release increased amounts of IL-6 or TNFα (139–142). Therefore, the potential relationship between macrophages and the changes in the systemic APR following injection of charged MPIO should be fully investigated.

Macrophages are versatile cells that are highly specialized in removing cell debris or presenting antigens for immune response initiation. Most macrophages differentiated from circulating monocytes, are present in the tissues, and are distinguished from dendritic cells by their expression of F4/80, CD11b and Fc receptors. They can be further subcategorized into subpopulations based on their anatomical location and functional phenotype (143), including osteoclasts (bone resident), microglia (brain resident), alveolar macrophages (lung resident) histiocytes (interstitial connective tissue resident) and Kupffer cells (liver resident); among these, Kupffer cells comprise the largest population of resident tissue macrophages in the body. Kupffer cells play a critical role in the innate immune response by efficiently phagocytosing pathogens along hepatic sinusoid endothelium, and some subtypes of Kupffer cell express a higher level of pro-inflammatory cytokines, such as TNFα, IL-6 and IL-12, when activated (144). MPIOs are mainly sequestered by the liver and spleen with this process beginning 30 min after their injection (98). Moreover, it is clear from the results presented in this thesis that the hepatic, not splenic, APR at T = 4 h was affected by the injection of charged MPIOs. Considering the irreplaceable role of the liver in systemic inflammation and the cytotoxicity of particles on macrophages, it is hypothesized that Kupffer cells are the

main targets of charged MPIOs *in vivo*. Such targeting may be mediated by electrostatic interactions between cellular and MPIO surfaces. By engulfing these particles and subsequently undergoing apoptosis, Kupffer cells could lose their ability to respond to immune signals from the CNS, causing suppression of the hepatic APR and neutrophil recruitment.

Several possible experiments could be used to test the aforementioned hypothesis *in vivo*. For example, to obtain direct evidence of Kupffer cell-induced MPIO endocytosis *in vivo,* fluorescence imaging could be used to investigate the overlap between Kupffer cells and fluorescent MPIOs in liver tissue slices, or toluidine blue staining of semi-thin slices could be used as a simpler alternative (41). The importance of Kupffer cells in responding to charged particles could be demonstrated by clodronate-induced macrophage depletion (144), in order to observe whether animals treated in advance by intravenous injection of clodronate liposomes have different levels of hepatic APR. In addition, live imaging of Kupffer cells after particle injection could be achieved using ligand-based PET. Translocator protein-18kDa (TSPO) is a cholesterol translocator on the outer mitochondrial membrane of activated macrophages/microglia (145). To investigate whether apoptosis of macrophages is mediated by charged MPIOs, radioactive TSPO ligands, such as [^{11}C] PK11195 (146), could be used to measure non-invasively the density of Kupffer cells and microglia at different time points after amine-MPIO injection. Furthermore, as other chemokines, such as CCL3, have also been reported to decrease after clodronate injection (147), their potential changes following amine-MPIO injection should also be investigated.

The downregulation of TNFα, CXCL10, CCL2 and E-selectin in the liver by amine-MPIOs revealed by the present results suggests that some contrast agents have the potential to modify the inflammatory process. Previous studies of the functions of Kupffer cells in IL-1β-induced acute brain injury showed a similar decrease of hepatic CXCL10 and CCL2 after

clodronate-mediated Kupffer cell depletion (148), implying Kupffer cells as the target of the charged particles. However, the hepatic level of IL-1β after Kupffer cell depletion was significantly reduced, while hepatic neutrophil recruitment was unchanged, when Kupffer cells were depleted. These systemic inflammatory responses thus differ from the cellular and molecular changes identified in this study after amine-MPIO injection. Therefore, cells other than Kupffer cells may also be involved as the *in vivo* target of amine-MPIOs.

The real-time PCR experiments described in the present study revealed that of the inflammatory mediators tested, TNFα and CCL2 decreased in both the liver and spleen. These two cytokines are produced predominantly by macrophages during the early stages of infection, with TNFα considered a hallmark of acute and chronic neuroinflammation in MS, ischaemic stroke, Parkinson's disease and Alzheimer's disease (149–151). Strikingly, TNFα is only upregulated in the liver, and not in the brain, after IL-1β-induced brain lesions, indicating that hepatic TNFα is an important amplifier for the central inflammation and systemic leukocyte recruitment (112). In a previous experiment carried out in my host laboratory, intravenous injection of the TNFα inhibitor, etanercept (which functions as a decoy receptor that binds endogenous TNF), in the IL-1β-mediated model of brain injury led to a suppression of both neutrophil recruitment and hepatic expression of CCL2 (152). This discovery reminds us that TNFα downregulation could potentially trigger a decrease in other APPs after amine-MPIO injection. Therefore, the mechanism underlying the suppression of TNFα expression should be elucidated as a priority, before other investigations are carried out on a molecular level. As CCL2 plays a key role in the regulation of monocyte and neutrophil recruitment (153), it is assumed that amine-MPIOs initially inhibit systemic inflammation by inducing the apoptosis of Kupffer cells. Such apoptosis then suppresses the hepatic secretion of CCL2 by reducing the amount of TNFα from Kupffer cells. To test this

hypothesis, selective agonists of the TNF receptor could be injected intravenously with amine-MPIOs for systemic modulation.

CCL2 is produced by many cell types, including endothelial cells, fibroblasts, macrophages and smooth muscle (154). These cells are important for immune responses in the peripheral circulation and tissues, with macrophages being the major source of CCL2 (155). In the CNS, CCL2 is produced predominately by astrocytes and resident microglia, and to a lesser extent by endothelial cells (156). *In vitro* and *in vivo* assays have shown that CCL2 expression is triggered during the inflammatory response by stimuli such as IL-1β, TNFα, LPS and interferons, and that this leads to macrophage activation (157–158). Moreover, CCL2 has been discovered to induce monocyte infiltration and leukocyte accumulation in the CNS. This acceleration of cerebral inflammation is mediated either by CCL2-CCR2 interactions along the activated endothelium (159), or by the direct effect of CCL2 on BBB permeability (160). As the hepatic CCL2 level is suppressed by amine-MPIOs, the circulating CCL2 level, the number of circulating monocytes, and the density of CNS-infiltrating monocytes may also theoretically be affected by the injection of charged particles. These parameters could be measured by flow cytometry or immunostaining using antibodies against CD11b, Iba-1 or CD45.

Despite evidence showing a detrimental effect of TNFα- and CCL2-mediated signalling to accelerate inflammation, these two APPs can also produce beneficial effects on immune responses at both the cellular and physiological level. The dual roles of these molecules are illustrated, for example, by the disappointing results of anti-TNFα therapies in patients with inflammatory diseases (161). TNFα can induce cellular proliferation, migration, differentiation or apoptosis, depending on the circumstances. With regard to the detrimental actions, TNFα induces the expression of various genes that are involved in cell infiltration, such as adhesion molecules, urokinase plasminogen activator (UPA), matrix

metalloproteinase 9 (MMP9), and vascular endothelial growth factor (VEGF). In addition, overexpression of TNFα leads to demyelinating disease, and neutralization of TNFα with antibodies has been shown to be protective in a mouse model of experimental autoimmune encephalomyelitis (EAE) (162). With regard to the beneficial part, the deletion of TNFα induces increased susceptibility to microbial infection, indicating a crucial role of TNFα in the protection against infection. It has also been demonstrated that administration of a low dose of TNFα can reduce the extent of myocardial infarction (163), or inhibit the apoptosis of leukocytes that are crucial for the maintenance of the immune system (164). Similarly, CCL2 possesses detrimental and pleiotropic effects at different stages of inflammation. Detrimentally, CCL2 mediates leukocyte adhesion to brain parenchyma by upregulating ICAM expression in the early stages of traumatic brain injury (TBI) (165). CCL2 KO mice exhibit smaller cortical lesions, reduced neuronal loss, and diminished macrophage accumulation compared to WT mice after TBI, indicating that CCL2 elevation is an important response in acute brain inflammation (166). On the other hand, a neuroprotective role of CCL2 has been revealed in studies of adult neurogenesis in models of stroke (167). It is now well recognized that immune inhibition may lead to short-term beneficial effects, following by long-term detrimental effects. Therefore, it will be important to elucidate the long-term pharmacological effects of charged MPIOs on systemic inflammation, using real-time PCR and immunostaining in the period T = 6–24 h, in order to avoid any potential adverse effects of these agents before they are applied in a clinical setting.

The IL-1- and IL-6-type cytokine families are the leading regulators of the APR in hepatocytes and the main mediators between cerebral and peripheral inflammation. These cytokines are produced mainly by macrophages and monocytes, and regulate the production of cytokines, adhesion molecules, glucocorticoids and growth factors. IL-1-type cytokines include IL-1α and IL-1β, and are expressed at very low levels in the adult healthy brain. At

the onset of inflammation, IL-1-type cytokines activate pathways involving nuclear factor kappa-B (NF-κB), c-Jun N-terminal kinase (JNK) and extracellular-signal regulated kinase (ERK1/2). IL-6-type cytokines include IL-6, leukaemia inhibitory factor (LIF), IL-11 and cardiotrophin-1 (CT-1), and specifically activate the JAK-STAT3 pathway. Both IL-1β and IL-6, for example, have been found to stimulate hepatic APP secretion (168). While some APPs, such as CRP and haptoglobin, are synergistically regulated by IL-1β and IL-6 (class I), others, including fibrinogens and α_2-macroglobulin, are solely responsive to IL-6-type cytokines (class II). The finding (in the present study) that injection of amine-MPIOs suppressed hepatic IL-6 expression but not IL-1β expression suggests that it will be important to investigate the hepatic expression of class II APPs in the future. Furthermore, it will also be necessary to directly measure the activation of NF-κB or STAT3 in macrophages cultured with amine-MPIOs, using Western blotting or ELISA techniques, as a step toward elucidating the molecular pathways modulated by these charged particles.

The decrease in splenic CXCL10 after injection of amine-MPIOs implies that the systemic recruitment of macrophages may be suppressed by charged particles, as CXCL10 performs homing functions in macrophages, dendritic cells and activated T lymphocytes. CXCL10 is secreted by leukocytes, neutrophils, monocytes and endothelial cells that are induced by interferon-γ (IFN-γ) during inflammation (169–170). It specifically activates CXCR3 and attracts CXCR3-positive cells, such as macrophages, to inflamed sites. In addition, CXCL10 has also been identified in astrocytes, microglia and neurons, with its expression level regulated by IL-1β and TNFα (171–172). As charged MPIOs were not found to be distributed in the brain parenchyma (by MRI or Prussian blue staining), it is assumed that these particles will not affect CXCL10 levels in the CNS in the short term. Based on this, we may observe a smaller change in the macrophage/monocyte density in brain parenchyma than that seen in the liver and spleen at various time points after injection of amine-MPIOs.

However, this assumption is also dependent on expressional changes in other CXCR3 ligands, including CXCL9 and CXCL11. These possibilities merit further investigation.

Pathways involving COX enzymes clearly play an important role in neuroinflammation, and these can be modulated by growth factors, IL-1β, TNFα and LPS (173). The observed decrease in hepatic COX-1 level in response to injection of amine-MPIOs correlated with the pattern of inhibition of cytokines and chemokines, while the upregulation of hepatic COX-2 by carboxylic acid-coated MPIOs revealed, for the first time, an ability of negatively charged particles to regulate systemic inflammation. Although COX-1 and COX-2 share 60% homology in their amino acid sequences, these two isoforms differ substantially in their regulatory mechanisms and tissue distributions. At the sequencing level, the COX-1 promoter contains several SP1 elements with a high GC content, while the COX-2 gene has a TATA box and a CAAT enhancer binding protein beta (C/EBP β) sequence (174). Both isoforms are constitutively expressed in the brain, with COX-1 expressed mainly in microglia and COX-2 in post-synaptic terminals (175). During the process of neuroinflammation, it is likely that COX-1 is an accelerator of immune responses, while COX-2 may mediate an anti-inflammatory role depending on the stimulus. For instance, in a model of intracerebroventricular LPS-induced neuroinflammation, neutrophil recruitment and microglial activation in the brain were attenuated in COX-1 KO mice, but increased in COX-2 KO mice. Moreover, plasma and brain CCL2 levels were found to be positively correlated with the COX-1 level, but negatively correlated with the COX-2 level; this would be consistent with the change in the APR observed after the injection of charged particles (176). In addition, COX-1 inhibition has been reported to attenuate the BBB disruption that occurs in TNFα- or LPS-induced neuroinflammation, whereas COX-2 gene deletion has been found to increase the permeability of the BBB (176–177). Considering the differential functions of COX-1 and COX-2 during inflammation, the relationships between these two isoforms and

charged particles should be investigated further. COX-2 should be chosen as the core target of further research, because to date it is the only APP reported to be modulated by carboxylic acid-coated MPIOs.

The long-term (T = 6–24 h) pharmacological effects of coated MPIOs *in vivo*, including actions on systemic inflammation in the liver and brain, the bio-distribution of these MPIOs, and the toxicities of iron oxide particles, have yet to be determined. Leukocyte recruitment to an injured CNS has been found to be delayed compared with the periphery (106), suggesting that the potential effects of coated MPIOs on cerebral leukocyte recruitment should be studied at time points later than 12 h after IL-1β injection. As an extension of the current project, the temporal and spatial distributions of coated MPIOs will be measured in the periphery between T = 6 h and T = 24 h. Unpublished data from my host laboratory reveals that MRI signals do not remain near CNS inflammatory lesion sites 5 h after injection of Lewis antigen-coated MPIO, possibly due to MPIOs breaking away from the luminal surface of endothelial cells into the circulation. However, a large number of MPIOs still exists in the liver and spleen at T = 24 h. Based on the above observations, the peripheral system is more likely to be influenced by MPIOs in the long term than the CNS.

Following the completion of comprehensive studies of the effects of coated MPIOs after IL-1β-induced acute brain injury, these coated MPIOs can be applied for the imaging of more complex inflammation. Intravenous injection of LPS and controlled cortical impact (CCI) represent alternative models of acute brain inflammation, while animal models, such as adenovirus-mediated IL-1β expression, EAE and MCAO, can replicate certain neuropathological components or phases that prevail in human disorders; these are thus ideal platforms to test the safety and functions of targeted MPIOs for further application. As Lewis antigen-decorated MPIOs are electrically neutral in the circulation, adding charged residues

to these particles may allow for optimization of their imaging contrast properties or even modulation of the inflammatory process in complex models.

Many physical characteristics of iron oxide particles, including their surface charge, crystallinity, smoothness and hydrophobicity/hydrophilicity, are important for their *in vivo* application. These factors have been shown to determine the residence time of iron oxide particles in the circulatory system (178). Moreover, iron oxide particles with a positive charge show higher internalization into human breast cancer cells than negatively charged particles, whereas no difference is found in the degree of internalization into HUVECs (176); this indicates that the pattern of MPIO uptake depends not only on the surface properties but also on the cell type. The physical properties of particles also affect their opsonisation process. It is concluded that the larger the size and the higher the hydrophobicity of the particles, the more efficient the opsonisation process will be (177). Thus, adding some hydrophobic groups along with Lewis antigens on the surface of MPIOs might be another method to enhance the ability of iron oxide particles to adhere to activated endothelium.

Surface modification of MPIOs can be carried out either during their synthesis or in a post-synthesis process. The ideal molecules used for stabilization of iron oxide particles should be biocompatible and biodegradable. However, some of the molecules commonly used are not biodegradable and have the potential to be improved. Most of these molecules are polymers, silica and organic dye molecules (Table 3) that protect the core against oxidation (179–192). For example, polystyrene is a widely used coating, applied to iron oxide using divinylbenzene as a cross-linker (193). Several other polymers, such as PLA, PEG, polyvinyl alcohol (PVA) and starch, are also used as coating materials. Some groups have prepared PEG-coated particles functionalized with a mannose-based analogue for targeting TNFα-stimulated E-selectin-expressing HUVECs (194). As a PEG coating is found to inhibit protein adsorption or reduce the efficiency of antibody coupling (195), the chemical

composition of the shell should be carefully selected to maximize the binding affinity of the iron oxide particles to inflamed sites.

Table 3. Materials used for coating iron oxide particles and related applications.

Coating material	Applications	Advantages	Ref.
Polyethylene glycol (PEG)	*In vivo* MRI	Improves the biocompatibility, blood circulation time and internalization efficiency of particles, easy to functionalise	(181)
Polyvinyl alcohol (PVA)	*In vivo* MRI and drug delivery	Prevents coagulation of particles	(182)
Polyvinyl pyrrolidine (PVP)	*In vivo* MRI and drug delivery	Enhances the blood circulation time and stabilises the colloidal solution	(183)
Polyacrylic acid	Target thrombolysis with recombinant tissue plasminogen activator	Increases the stability and biocompatibility of the particles	(184)
Polystyrene	*In vivo* MRI	Maintains stable and uniform-sized particles in suspension	(185)
Polymethyl methaacrylate	DNA separation and amplification	Can be applied in automatic systems for high-throughput detection of single nucleotide polymorphisms	(186)

Ethyl cellulose	Extraction of pharmaceutical chemicals	Enhances drug absorption into surrounding tissues	(187)
Chitosan	*In vivo* MRI and drug delivery	Biocompatible and hydrophilic (cationic)	(188)
Dextran	*In vivo* MRI and drug delivery	Enhances the blood circulation time and stabilizes the colloidal solution	(189)
Starch	*In vivo* MRI	Biocompatible and biodegradable	(190)
Albumin	Cell separation	Magnetic tagging and separation, does not affect cell viability and proliferation	(191)
Gelatin	Drug delivery	Hydrophilic and biocompatible, improves the efficiency of antigen loading	(192)

Extensive *in vitro* assays in various cell types and *in vivo* toxicity assays have been conducted to probe the possible cytotoxicity of both bare and coated iron oxide particles, due to their increasing presence in biomedical applications (Table 4) (196–206). After modification to avoid interference by cell media, these methods can also be employed for the toxicological study of the coated MPIOs used in the present study. USPIOs have been most thoroughly investigated because of their longer blood circulation time compared with MPIOs, and the majority of results to date have shown little toxicity (201). However, in some studies, USPIOs have been reported to arrest the cell cycle in the G_0G_1 cell-life gap, which may have been caused by related autophagy (207); this raises the possibility that MPIOs may have similar adverse effects. In addition to the cell-particle interactions, it is now well recognized that the adsorption of proteins by iron oxide particles *in vivo* may also have significant impacts on biological, biochemical and cellular behaviour, and this may be a key feature defining the toxicity of these particles (204). Unfavourable changes in protein configuration, mediated by protein-particle interactions, can lead to fibrillation, loss of function, or even the initiation of a new immune response due to the exposure of new antigenic sites (208). Size-exclusion chromatography (SEC) and surface plasmon resonance (SPR) are possible approaches to investigate such interactions. SEC allows study of the affinity of protein bonding to particles, while SPR measures the rates of protein association and disassociation (209). By applying some of the methods mentioned above, the toxicological effects of Lewis antigen-coated MPIOs and charged MPIOs can be thoroughly investigated.

Table 4. Methods used to evaluate the toxicity of iron oxide particles.

Cytotoxicity evaluation methods	Coating	Conclusion	Ref.
MTT assay	PEG, PEGF, PVA, silica, dextran, PEI, and chitosan	No toxicity is observed even at a high applied dosage	(196)
Modified MTT assay	PEGF and PVA	The toxicity of iron oxide particles is observed when the surface is saturated	(197)
Redox assay	Dextran, oleate and PEI	The iron oxide particles are stable in a variety of media and show no toxicity during interaction with various cells	(198)
Cytochrome c assay	Amine-functionalized	Low cytotoxicity of amine-coated iron oxide particles on some liver cells	(199)
Nitroblue tetrazolium assay	Dextran	No significant cytotoxicity	(200)
WST assay	Dextran	No detectable cytotoxicity	(201)

Lactate dehydrogenase assay	None	Bare iron oxide particles show no toxicity	(202)
Various dyes	None, dextran and PVA	No cytotoxicity; a trace of apoptosis is detected for the bare iron oxide particles	(203)
Cell cycle assay	None and PVA	PVA-coated iron oxide particles show no necrosis, apoptosis or cell cycle arrest at moderate concentrations of particles, while at high concentrations, these coated particles cause both apoptosis and cell cycle arrest	(204)
[^{3}H]-thymidine assay	Gold	No detectable cytotoxicity	(205)
Comet assay	None	Oxidative DNA lesions are observed after exposure to high concentrations of iron oxide particles	(206)

Abbreviations: DNA, deoxyribonucleic acid; MTT, 3-[4,5-dimethylthiazol-2-yl]-2,5 diphenyl tetrazolium bromide; PEG, polyethylene glycol; PEGF, poly-(ethylene glycol)-co-fumarate; PEI, polyethylenimine; PVA, polyvinyl alcohol; WST, water-soluble tetrazolium salt.

The diagnostic and potential therapeutic applications of iron oxide particles in CNS inflammation are currently undergoing a rapid growth. Since the first report of using USPIOs as MRI contrast agents in 1990 (210), more particles have been designed for the molecular imaging of inflamed sites as well as cell trafficking. Macrophage infiltration and microglial activation are prominent at the periphery of brain lesions. It has been feasible to label these macrophages to track their migration in the brain or circulation (29). Moreover, by using iron oxide particles and T_2*-weighted imaging in experimental stroke models, it has been possible to differentiate inflamed from non-inflamed infarct subareas that could not be differentiated by Gd chelates and perfusion-weighted MRI (211). The potential applicability of iron oxide particle-enhanced MRI in human brain imaging has been studied in patients with stroke and MS (212–213), and these investigations have revealed that Gd chelates and iron oxide particles show distinct areas of signal enhancement. This clinical research has provided solid evidence that iron oxide particles are at the very least useful as supplements to Gd chelates for MRI. With regard to their further development through conjugation to low molecular weight ligands, peptides and polysaccharides, these iron oxide particles will evidently increase our understanding of the early processes occurring in many neurological disorders, from the molecular to the pathological level.

Conclusion

We used MRI data to find that unsialated Le^A-MPIOs specifically accumulated in the inflamed sites in mice and rat injury models during the early stage of CNS inflammation. Immunostaining and Prussian blue staining confirmed such results in the tissue level, and also revealed that these type I Lewis sugar-coated MPIOs bound to endothelium-like structures. BBB was disrupted by Le^A-MPIO injection from results of IgG and neutrophil staining. Furthermore, LeB-MPIOs only showed MRI signal enhancement in rat brains, not in mouse

brains. On the other hand, the investigation on pharmacological effect of charged MPIOs showed that only positive-charged MPIOs led to the suppression on systemic APR and hepatic neutrophil recruitment within short-term time scale. Such discoveries are essential for the potential application of carbohydrate-coated MPIOs in the future, suggesting that there is still much to do for the development of next-generation MRI agents.

References

1. Frijns, C.J., Kappelle, L.J. Inflammatory cell adhesion molecules in ischaemic cerebrovascular disease. Stroke 33, 2115–2122 (2002).
2. Okada, Y., Copeland, B.R., Mori, E., et al. P-selectin and intercellular adhesion molecule-1 expression after focal brain ischaemia and reperfusion. Stroke 25, 202–211 (1994).
3. Dorey, E., Chang, N., Liu, Q.Y., et al. Apolipoprotein E, amyloid-beta, and neuroinflammation in Alzheimer's disease. Neurosci Bull (2014), in press.
4. Choudhury, R.P., Fuster, V., Fayad, Z.A. Molecular, cellular and functional imaging of atherothrombosis. Nat Rev Drug Discov 3, 913–925 (2004).
5. Dansky, H.M., Barlow, C.B., Lominska, C., et al. Adhesion of monocytes to arterial endothelium and initiation of atherosclerosis are critically dependent on vascular cell adhesion molecule-1 gene dosage. Arterioscler Thromb Vasc Biol 21, 1662–1667 (2001).
6. D'Mello, C., Swain, M.G. Liver-brain inflammation axis. Am J Physiol Gastrointest Liver Physiol 301, 749–761 (2011).
7. Navarro-González, J.F., Mora-Fernández, C., Muros de Fuentes, M., et al. Inflammatory molecules and pathways in the pathogenesis of diabetic nephropathy. Nat Rev Nephrol 7, 327–340 (2011).
8. Ransohoff, R.M., Kivisakk, P., Kidd, G. Three or more routes for leukocyte migration into the central nervous system. Nat Rev Immunol 3, 569–581 (2003).
9. Abbott, N.J., Ronnback, L., Hansson, E. Astrocyte-endothelial interactions at the blood-brain barrier. Nat Rev Neurosci 7, 41–53 (2006).

10. Nagy, Z., Peters, H., Huttner, I. Fracture faces of cell junctions in cerebral endothelium during normal and hyperosmotic conditions. Lab Invest 50, 313–322 (1984).

11. Kivisakk, P., Mahad, D.J., Callahan, M.K., et al. Human cerebrospinal fluid central memory CD4+ T cells: evidence for trafficking through choroid plexus and meninges via P-selectin. Proc Natl Acad Sci USA 100, 8389–8394 (2003).

12. Rudd, J.H., Hyafil, F., Fayad, Z.A. Inflammation imaging in atherosclerosis. Arterioscler Thromb Vasc Biol 29, 1009–1016 (2009).

13. Tahara, N., Kai, H., Ishibashi, M., et al. Simvastatin attenuates plaque inflammation: evaluation by fluorodeoxyglucose positron emission tomography. J Am Coll Cardiol 48, 1825–1831 (2006).

14. Sipkins, D.A., Cheresh, D.A., Kazemi, M.R., et al. Detection of tumor angiogenesis in vivo by alphaVbeta3-targeted magnetic resonance imaging. Nat Med 4, 623–626 (1998).

15. Yu, X., Song, S.K., Chen, J., et al. High-resolution MRI characterization of human thrombus using a novel fibrin-targeted paramagnetic nanoparticle contrast agent. Magn Reson Med 44, 867–872 (2000).

16. Lim, Y.L., Lee, H.Y., Low, S.C., et al. Possible role of gadolinium in nephrogenic systemic fibrosis: report of two cases and review of the literature. Clin Exp Dermatol 32, 353–358 (2007).

17. Stratta, P., Canavese, C., Aime, S. Gadolinium-enhanced magnetic resonance imaging, renal failure and nephrogenic systemic fibrosis/nephrogenic fibrosing dermopathy. Curr Med Chem 15, 1229–1235 (2008).

18. Neuwelt, E.A., Hamilton, B.E., Varallyay, C.G., et al. Ultrasmall superparamagnetic iron oxides (USPIOs): a future alternative magnetic resonance (MR) contrast agent

for patients at risk for nephrogenic systemic fibrosis (NSF)? Kidney Int 75, 465–474 (2008).

19. Kuntz, E., Kuntz, H.D.. Hepatology: Principles and Practice: History, Morphology, Biochemistry, Diagnostics, Clinic, Therapy (2nd Edition). Springer, 19-24 (2006).

20. Manninger, S.P., Muldoon, L.L., Nesbit, G., et al. An exploratory study of ferumoxtran-10 nanoparticles as a blood-brain barrier imaging agent targeting phagocytic cells in CNS inflammatory lesions. AJNR Am J Neuroradiol 26, 2290–2300 (2005).

21. Saleh, A., Schroeter, M., Ringelstein, A., et al. Iron oxide particle enhanced MRI suggests variability of brain inflammation at early stages after ischaemic stroke. Stroke 38, 2733–2737 (2007).

22. Vellinga, M.M., Oude Engberink, R.D., Seewann, A., et al. Pluriformity of inflammation in multiple sclerosis shown by ultra-small iron oxide particle enhancement. Brain 131, 800–807 (2008).

23. Neuwelt, E.A., Varallyay, C.G., Manninger, S., et al. The potential of ferumoxytol nanoparticle magnetic resonance imaging, perfusion, and angiography in central nervous system malignancy: a pilot study. Neurosurgery 60, 601–611 (2007).

24. Rausch, M., Hiestand, P., Baumann, D., et al. MRI-based monitoring of inflammation and tissue damage in acute and chronic relapsing EAE. Magn Reson Med 50, 309–314 (2003).

25. Rausch, M., Hiestand, P., Foster, C.A., et al. Predictability of FTY720 efficacy in experimental autoimmune encephalomyelitis by in vivo macrophage tracking: clinical implications for ultrasmall superparamagnetic iron oxide-enhanced magnetic resonance imaging. J Magn Reson Imaging 20, 16–24 (2004).

26. Thorek, D.L., Chen, A.K., Czupryna, J., et al. Superparamagnetic iron oxide nanoparticle probes for molecular imaging. Ann Biomed Eng 34, 23–38 (2006).

27. Tabata, Y., Ikada, Y. Phagocytosis of polymer microspheres by macrophages. Adv Polym Sci 94, 107–141 (1990).

28. McAteer, M.A., Akhtar, A.M., von Zur Muhlen, C., et al. An approach to molecular imaging of atherosclerosis, thrombosis, and vascular inflammation using microparticles of iron oxide. Atherosclerosis 209, 18–27 (2010).

29. Tabata, Y., Ikada, Y. Effect of the size and surface charge of polymer microspheres on their phagocytosis by macrophage. Biomaterials 9, 356–362 (1988).

30. Briley-Saebo, K.C., Johansson, L.O., Hustvedt, S.O., et al. Clearance of iron oxide particles in rat liver: effect of hydrated particle size and coating material on liver metabolism. Invest Radiol 41, 560–571 (2006).

31. Morris, J.B., Olzinski, A.R., Bernard, R.E., et al. p38 MAPK inhibition reduces aortic ultrasmall superparamagnetic iron oxide uptake in a mouse model of atherosclerosis: MRI assessment. Arterioscler Thromb Vasc Biol 28, 265–271 (2008).

32. Muldoon, L.L., Varallyay, P., Kraemer, D.F., et al. Trafficking of superparamagnetic iron oxide particles (Combidex) from brain to lymph nodes in the rat. Neuropathol Appl Neurobiol 30, 70–79 (2004).

33. Yang, Y., Yanasak, N., Schumacher, A., et al. Temporal and noninvasive monitoring of inflammatory-cell infiltration to myocardial infarction sites using micrometer-sized iron oxide particles. Magn Reson Med 63, 33–40 (2010).

34. Ye, Q., Wu, Y.L., Foley, L.M., et al. Longitudinal tracking of recipient macrophages in a rat chronic cardiac allograft rejection model with noninvasive magnetic resonance imaging using micrometer-sized paramagnetic iron oxide particles. Circulation 118, 149–156 (2008).

35. Varallyay, P., Nesbit, G., Muldoon, L.L., et al. Comparison of two superparamagnetic viral-sized iron oxide particles ferumoxides and ferumoxtran-10 with a gadolinium chelate in imaging intracranial tumors. AJNR Am J Neuroradiol 23, 510–519 (2002).

36. Matuszewski, L., Persigehl, T., Wall, A. Cell tagging with clinically approved iron oxides: feasibility and effect of lipofection, particle size, and surface coating on labeling efficiency. Radiology 235, 155–161 (2005).

37. Metz, S., Bonaterra, G., Rudelius, M., et al. Capacity of human monocytes to phagocytose approved iron oxide MR contrast agents in vitro. Eur Radiol 14, 1851–1858 (2004).

38. Brodbeck, W.G., Voskerician, G., Ziats, N.P., et al. In vivo leukocyte cytokine mRNA responses to biomaterials are dependent on surface chemistry. J Biomed Mater Res 64, 320–329 (2003).

39. Brodbeck, W.G., Patel, J., Voskerician, G. et al. Biomaterial adherent macrophage apoptosis is increased by hydrophilic and anionic substrates in vivo. Proc Natl Acad Sci USA 99, 10287–10292 (2002).

40. Spragg, D.D., Alford, D.R., Greferath, R., et al. Immunotargeting of liposomes to activated vascular endothelial cells: a strategy for site-selective delivery in the cardiovascular system. Proc Natl Acad Sci USA 94, 8795–8800 (1997).

41. Olivier, V., Riviere, C., Hindie, M., et al. Uptake of polystyrene beads bearing functional groups by macrophages and fibroblasts. Colloids Surf B Biointerfaces 33, 23–31 (2004).

42. Lomakina, E., Knauf, P.A., Schultz, J.B., et al. Activation of human neutrophil Mac-1 by anion substitution. Blood Cells Mol Dis 42, 177–184 (2009).

43. Enochs, W.S., Weissleder, R. MR imaging of the peripheral nervous system. J Magn Reson Imaging 4, 251–257 (1994).

44. Zhao, M., Beauregard, D.A., Loizou, L., et al. Non-invasive detection of apoptosis using magnetic resonance imaging and a targeted contrast agent. Nat Med 7, 1241–1244 (2001).

45. Pirko, I., Johnson, A., Ciric, B., et al. In vivo magnetic resonance imaging of immune cells in the central nervous system with superparamagnetic antibodies. FASEB 18, 179–182 (2004).

46. Wadghiri, Y.Z., Sigurdsson, E.M., Sadowski, M., et al. Detection of Alzheimer's amyloid in transgenic mice using magnetic resonance microimaging. Magn Reson Med 50, 293–302 (2003).

47. Renshaw, P.F., Owen, C.S., Evans, A.E., et al. Immunospecific NMR contrast agents. Magn Reson Imaging 4, 351–357 (1986).

48. Funovics, M.A., Kapeller, B., Hoeller, C., et al. MR imaging of the her2/neu and 9.2.27 tumor antigens using immunospecific contrast agents. Magn Reson Imaging 22, 843–850 (2004).

49. Papisov, M.I., Bogdanov, A., Schaffer, B., et al. Colloidal magnetic resonance contrast agents: effect of particle surface on biodistribution. J Magn Magn Mater 122, 383–386 (1993).

50. Suwa, T., Ozawa, S., Ueda, M., et al. Magnetic resonance imaging of esophageal squamous cell carcinoma using magnetite particles coated with antiepidermal growth factor receptor antibody. Int J Cancer 75, 626–634 (1998).

51. Kang, H.W., Josephson, L., Petrovsky, A., et al. Magnetic resonance imaging of inducible E-selectin expression in human endothelial cell culture. Bioconjug Chem 13, 122–127 (2002).

52. Schellenberger, E.A., Bogdanov, A.J., Hogemann, D., et al. Annexin V-CLIO: a nanoparticle for detecting apoptosis by MRI. Mol Imaging 1, 102–107 (2002).

53. Tsourkas, A., Shinde-Patil, V.R., Kelly, K.A., et al. In vivo imaging of activated endothelium using an anti-VCAM-1 magnetooptical probe. Bioconjug Chem 16, 576–581 (2005).

54. van Kasteren, S.I., Campbell, S.J., Serres, S., et al. Glyconanoparticles allow pre-symptomatic in vivo imaging of brain disease. Proc Natl Acad Sci USA 106, 18–23 (2009).

55. Funovics, M., Montet, X., Reynolds, F., et al. Nanoparticles for the optical imaging of tumor E-selectin. Neoplasia 7, 904–911 (2005).

56. McAteer, M.A., Sibson, N.R., von Zur Muhlen, C., et al. In vivo magnetic resonance imaging of acute brain inflammation using microparticles of iron oxide. Nat Med 13, 1253–1258 (2007).

57. Hoyte, L.C., Brooks, K.J., Nagel, S., et al. Molecular magnetic resonance imaging of acute vascular cell adhesion molecule-1 expression in a mouse model of cerebral ischaemia. J Cereb Blood Flow Metab 30, 1178–1187 (2010).

58. Serres, S., Soto, M.S., Hamilton, A., et al. Molecular MRI enables early and sensitive detection of brain metastases. Proc Natl Acad Sci USA 109, 6674–6679 (2012).

59. Duffy, B.A., Choy, M., Riegler, J., et al. Imaging seizure-induced inflammation using an antibody targeted iron oxide contrast agent. Neuroimage 60, 1149–1155 (2012).

60. McAteer, M.A., Schneider, J.E., Ali, Z.A., et al. Magnetic resonance imaging of endothelial adhesion molecules in mouse atherosclerosis using dual-targeted microparticles of iron oxide. Arterioscler Thromb Vasc Biol 28, 77–83 (2008).

61. Alon, R., Feizi, T., Yuen, C.T., et al. Glycolipid ligands for selectins support leukocyte tethering and rolling under physiologic flow conditions. J Immunol 154, 5356–5366 (1995).

62. Stroud, M.R., Handa, K., Salyan, M.E.K., et al. Monosialogangliosides of human myelogenous leukemia HL60 cells and normal human leukocytes. 2. Characterization of E-selectin binding fractions, and structural requirements for physiological binding to E-selectin. Biochemistry 35, 770–778 (1996).

63. Wagers, A.J., Waters, C.M., Stoolman, L.M., et al. IL-12 and IL-4 control T cell adhesion to endothelial selectins through opposite effects on α1,3-fucosyltransferase VII gene expression. J Exp Med 188, 2225–2231 (1998).

64. Stanley, P., Cummings, R.D. Structures common to different glycans. In: Essentials of Glycobiology, 2nd Ed. Cold Spring Harbor Laboratory Press (2008).

65. Marcus, D.M., Cass, L.E. Glycosphingolipids with Lewis blood group activity: uptake by human erythrocytes. Science 164, 553–555 (1969).

66. Weissleder, R., Kelly, K., Sun, E.Y., et al. Cell-specific targeting of nanoparticles by multivalent attachment of small molecules. Nat Biotechnol 23, 1418–1423 (2005).

67. Sibson, N.R., Blamire, A.M., Bernades-Silva, M., et al. MRI detection of early endothelial activation in brain inflammation. Magn Reson Med 51, 248–252 (2004).

68. Barber, P.A., Foniok, T., Kirk, D., et al. MR molecular imaging of early endothelial activation in focal ischaemia. Ann Neurol 56, 116–120 (2004).

69. Boutry, S., Burtea, C., Laurent, S., et al. Magnetic resonance imaging of inflammation with a specific selectin-targeted contrast agent. Magn Reson Med 53, 800–807 (2005).

70. Minaguchi, J., Oohashi, T., Inagawa, K., et al. Transvascular accumulation of Sialyl Lewis X conjugated liposome in inflamed joints of collagen antibody-induced arthritic (CAIA) mice. Arch Histol Cytol 71, 195–203 (2008).

71. Ferrari, C.C., Depino, A.M., Prada, F., et al. Reversible demyelination, blood-brain barrier breakdown, and pronounced neutrophil recruitment induced by chronic IL-1 expression in the brain. Am J Pathol 165, 1827–1837 (2004).

72. Appelmelk, B.J., van Die, I., van Vliet, S.J., et al. Cutting edge: carbohydrate profiling identifies new pathogens that interact with dendritic cell-specific ICAM-3-grabbing non-integrin on dendritic cells. J Immunol 170, 1635–1639 (2003).

73. Soilleux, E.J. DC-SIGN (dendritic cell-specific ICAM-grabbing non-integrin) and DC-SIGN-related (DC-SIGNR): friend or foe? Clin Sci 104, 437–446 (2003).

74. Campbell, S.J., Deacon, R.M., Jiang, Y., et al. Overexpression of IL-1β by adenoviral-mediated gene transfer in the rat brain causes a prolonged hepatic chemokine response, axonal injury and the suppression of spontaneous behaviour. Neurobiol Dis 27, 151–163 (2007).

75. Borovikova, L.V., Ivanova, S., Zhang, M., et al. Vagus nerve stimulation attenuates the systemic inflammatory response to endotoxin. Nature 405, 458–462 (2000).

76. Campbell, S.J., Hughes, P.M., Iredale, J.P., et al. CINC-1 is an acute-phase protein induced by focal brain injury causing leukocyte mobilization and liver injury. FASEB J 17, 1168–1170 (2003).

77. Perry, V.H., Newman, T.A., Cunningham, C. The impact of systemic infection on the progression of neurodegenerative disease. Nat Rev Neurosci 4, 103–112 (2003).

78. Campbell. S.J., Perry, V.H., Butchart, A.G., et al. Central nervous system injury triggers hepatic CC and CXC chemokine expression that is associated with leukocyte mobilization and recruitment to both the central nervous system and the liver. Am J Pathol 166, 1487–1497 (2005).

79. Gris, D., Hamilton, E.F., Weaver, L.C. The systemic inflammatory response after spinal cord injury damages lungs and kidneys. Exp Neurol 211, 259–270 (2008).

80. Wilcockson, D.C., Campbell, S.J., Anthony, D.C., et al. The systemic and local acute phase response following acute brain injury. J Cereb Blood Flow Metab 22, 318–326 (2002).

81. Martin, R., McFarland, H.F., McFarlin, D.E. Immunological aspects of demyelinating diseases. Annu Rev Immunol 10, 153–187 (1992).

82. Sharkey, J., Ritchie, I.M., Kelly, P.A.T. Perivascular microapplication of endothelin-1: A new model for focal cerebral ischaemia in the rat. J Cereb Blood Flow Metab 13, 865–871 (1993).

83. Allan, S.M., Rothwell, N.J. Cytokines and acute neurodegeneration. Nat Rev Neurosci 2, 734–744 (2001).

84. Perry, V.H., Newman, T.A., Cunningham, C. The impact of systemic infection on the progression of neurodegenerative disease. Nat Rev Neurosci 4, 103–112 (2003).

85. Boutin, H., LeFeuvre, R.A., Horai, R., et al. Role of IL-1α and IL-1β in ischaemic brain damage. J Neurosci 21, 5528–5534 (2001).

86. Mann, C.L., Davies, M.B., Stevenson, V.L., et al. Interleukin 1 genotypes in multiple sclerosis and relationship to disease severity. J Neuroimmunol 129, 197–204 (2002).

87. de Jong, B.A., Huizinga, T.W., Bollen, E.L., et al. Production of IL-1β and IL-1Ra as risk factors for susceptibility and progression of relapse-onset multiple sclerosis. J Neuroimmunol 126, 172–179 (2002).

88. Loddick, S.A., Wong, M.L., Bongiorno, P.B., et al. Endogenous interleukin-1 receptor antagonist is neuroprotective. Biochem Biophys Res Commun 234, 211–215 (1997).

89. Grundy, R.I., Rothwell, N.J., Allan, S.M. Site-specific actions of interleukin-1 on excitotoxic cell death in the rat striatum. Brain Res 926, 142–148 (2002).

90. Hofman, F.M., Hinton, D.R., Johnson, K., et al. Tumor necrosis factor identified in multiple sclerosis brain. J Exp Med 170, 607–612 (1989).

91. Boka, G., Anglade, P., Wallach, D., et al. Immunocytochemical analysis of tumor necrosis factor and its receptors in Parkinson's disease. Neurosci Lett 172, 151–154 (1994).

92. Hallenbeck, J.M. The many faces of tumor necrosis factor in stroke. Nat Med 8, 1363–1368 (2002).

93. Selmaj, K., Raine, C.S., Cross, A.H. Anti-tumor necrosis factor therapy abrogates autoimmune demyelination. Ann Neurol 30, 694–700 (1991).

94. Probert, L., Akassoglou, K., Pasparakis, M., et al. Spontaneous inflammatory demyelinating disease in transgenic mice showing central nervous system-specific expression of tumor necrosis factor alpha. Proc Natl Acad Sci USA 92, 11294–11298 (1995).

95. Glabinski, A.R., Tuohy, V.K., Ransohoff, R.M. Expression of chemokines RANTES, MIP-1α and GRO-α correlates with inflammation in acute experimental autoimmune encephalomyelitis. Neuroimmunomodulation 5, 166–171 (1998).

96. Schnell, L., Fearn, S., Schwab, M.E., et al. Cytokine-induced acute inflammation in the brain and spinal cord. J Neuropathol Exp Neurol 58, 245–254 (1999).

97. Sibson, N.R., Blamire, A.M., Perry, V.H., et al. TNF-α reduces cerebral blood volume and disrupts tissue homeostasis via an endothelin- and TNFR2-dependent pathway. Brain 125, 2446–2459 (2002).

98. van Beers, B.E., Sempoux, C., Materne, R., et al. Biodistribution of ultrasmall iron oxide particles in the rat liver. J Magn Reson Imaging 13, 594–599 (2001).

99. von zur Muhlen, C., Peter, K., Ali, Z.A., et al. Visualization of activated platelets by targeted magnetic resonance imaging utilizing conformation-specific antibodies against glycoprotein IIb/IIIa. J Vasc Res 46, 6–14 (2009).

100. Bourrinet, P., Bengele, H.H., Bonnemain, B., et al. Preclinical safety and pharmacokinetic profile of ferumoxtran-10, an ultrasmall superparamagnetic iron oxide magnetic resonance contrast agent. Invest Radiol 41, 313–324 (2006).

101. Campbell, S.J., Anthony, D.C., Oakley, F., et al. Hepatic NF-κB regulates neutrophil recruitment to the injured brain. J Neuropathol Exp Neurol 67, 223–230 (2008).

102. Millward, J., Schnorr, J., Taupitz, M., et al. Iron oxide magnetic nanoparticles highlight early involvement of the choroid plexus in central nervous system inflammation. ASN Neuro 5, 89–98 (2013).

103. Fernández-López, D., Faustino, J., Daneman, R., et al. Blood–brain barrier permeability is increased after acute adult stroke but not neonatal stroke in the rat. J Neurosci 32, 9588–9600 (2012).

104. Blond, D., Campbell, S.J., Butchart, A.G., et al. Differential induction of interleukin-1beta and tumour necrosis factor-alpha may account for specific patterns of leukocyte recruitment in the brain. Brain Res 958, 89–99 (2002).

105. Paxinos, G., Watson, C. The Rat Brain in Stereotaxic Coordinates, 6th edition. Academic Press (2006).

106. Blond, D., Campbell, S.J., Butchart, A.G., et al. Differential induction of IL-1β and TNFα may account for specific patterns of leukocyte recruitment in the brain. Brain Res 958, 89–99 (2002).

107. Abdul, P.M., Alikunju, S., Szlachetka, A.M., et al. Impairment of brain endothelial glucose transporter by methamphetamine causes blood-brain barrier dysfunction. Mol Neurodegener 6, 23–35 (2011).

108. Chung, Y., Su, S., Huang, G., et al. Regulation of glucose transporter 1 by IL-1β stimulation in rat articular chondrocytes. J Med Sci 29, 125–130 (2009).

109. Cluitmans, F.H., Esendam, B.H., Landegent, J.E., et al. Constitutive in vivo cytokine and hematopoietic growth factor gene expression in the bone marrow and peripheral blood of healthy individuals. Blood 85, 2038–2044 (1995).

110. Salkeni, M.A., Lynch, J.L., Otamis-Price, T., et al. Lipopolysaccharide impairs blood-brain barrier P-glycoprotein function in mice through prostaglandin- and nitric oxide-independent pathways. J Neuroimmune Pharmacol 4, 276–282 (2009).

111. Verma, S., Nakaoke, R., Dohgu, S., et al. Release of cytokines by brain endothelial cells: a polarized response to lipopolysaccharide. Brain Behav Immun 20, 449–455 (2006).

112. Banks, W.A., Dohgu, S., Nakaoke, R., et al. Nitric oxide isoenzymes regulate LPS-enhanced insulin transport across the blood-brain barrier. Endocrinology 149, 1514–1523 (2008).

113. Murakami, H., Takanaga, H., Matsuo, H., et al. Comparison of blood-brain barrier permeability in mice and rats using in situ brain perfusion technique. Am J Physiol Heart Circ Physiol 279, 1022-1028 (2000).

114. Syvänen, S., Lindhe, O., Palner, M., et al. Species differences in blood-brain barrier transport of three positron emission tomography radioligands with emphasis on P-glycoprotein transport. Drug Metab Dispos 37, 635-643 (2009).

115. del Valle, J., Camins, A., Pallas, M., et al. A new method for determining blood-brain barrier integrity based on intracardiac perfusion of an Evans Blue-Hoechst cocktail. J Neurosci Methods 15, 42–49 (2008).

116. Raine, C.S., Cannella, B., Duijvestijn, A.M., et al. Homing to central nervous system vasculature by antigen-specific lymphocytes. II. Lymphocyte/endothelial cell adhesion during the initial stages of autoimmune demyelination. Lab Invest 63, 476–489 (1990).

117. Wolburg, H., Wolburg-Buchholz, K., Engelhardt, B. Diapedesis of mononuclear cells across cerebral venules during experimental autoimmune encephalomyelitis leaves tight junctions intact. Acta Neuropathol 109, 181–190 (2005).

118. Carman, C.V., Springer, T.A. Trans-cellular migration: cell-cell contacts get intimate. Curr Opin Cell Biol 20, 533–540 (2008).

119. Vestweber, D. Adhesion and signaling molecules controlling the transmigration of leukocytes through endothelium. Immunol Rev 218, 178–196 (2007).

120. Engelhardt, B., Wolburg, H. Mini-review: Transendothelial migration of leukocytes: through the front door or around the side of the house? Eur J Immunol 34, 2955–2963 (2004).

121. Hol, J., Kuchler, A.M., Johansen, F.E., et al. Molecular requirements for sorting of the chemokine IL-8/CXCL8 to endothelial Weibel-Palade bodies. J Biol Chem 284, 23532–23539 (2009).

122. Panzer, U., Steinmetz, O.M., Reinking, R.R., et al. Compartment-specific expression and function of the chemokine IP-10/CXCL10 in a model of renal endothelial microvascular injury. J Am Soc Nephrol 17, 454–464 (2006).

123. Kieseier, B.C., Tani, M., Mahad, D., et al. Chemokines and chemokine receptors in inflammatory demyelinating neuropathies: a central role for IP-10. Brain 125, 823–834 (2002).

124. Stamatovic, S.M., Keep, R.F., Kunkel, S.L., et al. Potential role of MCP-1 in endothelial cell tight junction ‘opening’: signaling via Rho and Rho kinase. J Cell Sci 116, 4615–4628 (2003).

125. Quandt, J., Dorovini-Zis, K. The beta chemokines CCL4 and CCL5 enhance adhesion of specific CD4+ T cell subsets to human brain endothelial cells. J Neuropathol Exp Neurol 63, 350–362 (2004).

126. Szczucinski, A., Losy, J. Chemokines and chemokine receptors in multiple sclerosis: potential targets for new therapies. Acta Neurol Scand 115, 137–146 (2007).

127. Pohlmann, S., Baribaud, F., Doms, R.W. DC-SIGN and DC-SIGNR: helping hands for HIV. Trends Immunol 22, 643–646 (2001).

128. Guo, Y., Feinberg, H., Conroy, E., et al. Structural basis for distinct ligand-binding and targeting properties of the receptors DC-SIGN and DC-SIGNR. Nat Struct Mol Biol 11, 591–598 (2004).

129. Garcia-Vallejo, J.J., van Liempt, E., da Costa Martins P., et al. DC-SIGN mediates adhesion and rolling of dendritic cells on primary human umbilical vein endothelial cells through LewisY antigen expressed on ICAM-2. Mol Immunol 45, 2359–2369 (2008).

130. Bogoevska, V., Nollau, P., Lucka, L., et al. DC-SIGN binds ICAM-3 isolated from peripheral human leukocytes through Lewis x residues. Glycobiology 17, 324–333 (2007).

131. Wu, L., Ramani, V.N. Dendritic-cell interactions with HIV: Infection and viral dissemination. Nat Rev Immunol 6, 859–868 (2006).

132. Powlesland, A.S., Ward, E.M., Sadhu, S.K., et al. Widely divergent biochemical properties of the complete set of mouse DC-SIGN-related proteins. J Biol Chem 281, 20440–20449 (2006).

133. Roser, M., Fischaer, D., Kissel, T. Surface-modified biodegradable albumin nano- and microspheres. II: effect of surface charges on in vitro phagocytosis and biodistribution in rats. Eur J Pharm Biopharm 46, 255–263 (1998).

134. Lück, M., Paulke, B.R., Schroder, W., et al. Analysis of plasma protein adsorption on polymeric nanoparticles with different surface characteristics. J Biomed Mater Res 39, 478–485 (1998).

135. Lück, M., Schroder, W., Paulke, B.R., et al. Complement activation by model drug carriers for intravenous application: determination by two-dimensional electrophoresis. Biomaterials 20, 2063–2068 (1999).

136. Tomazic-Jezic, V.J., Merritt, K., Umbreit, T.H. Significance of the type and the size of biomaterial particles on phagocytosis and tissue distribution. J Biomed Mater Res 55, 523–529 (2001).

137. Yamamoto, N., Fukai, F., Ohshima, H., et al. Dependence of the phagocytic uptake of polystyrene microspheres by differentiated HL60 upon the size and surface properties of the microspheres. Colloids Surf B 25, 157–162 (2002).

138. Olivier, V., Duval, J.L., Hindié, M., et al. Comparative particle-induced cytotoxicity toward macrophages and fibroblasts. Cell Biol Toxicol 19, 145–159 (2003).

139. Trindade, M.C., Lind, M., Nakashima, Y., et al. Interleukin-10 inhibits polymethylmethacrylate particle induced interleukin-6 and tumor necrosis factor-alpha release by human monocyte/macrophages in vitro. Biomaterials 22, 2067–2073 (2001).

140. Algan, S.M., Purdon, M. Horowitz, S.M. Role of tumor necrosis factor alpha in particulate-induced bone resorption. J Orthop Res 14, 30–35 (1996).

141. Catelas, I., Petit, A., Marchand, R., et al. Cytotoxicity and macrophage cytokine release induced by ceramic and polyethylene particles in vitro. J Bone Joint Surg Br 81, 516–521 (1999).

142. Ma, N., Petit, A., Yahia, L., et al. Cytotoxic reaction and TNF-α response of macrophages to polyurethane particles. J Biomater Sci Polym Ed 13, 257–272 (2002).

143. Gordon, S., Taylor, P.R. Monocyte and macrophage heterogeneity. Nat Rev Immunol 5, 953–964 (2005).

144. Daneneberg, H.D., Fishbein, I., Gao, J., et al. Macrophage depletion by clodronate-containing liposomes reduces neointimal formation after balloon injury in rats and rabbits. Circulation 106, 599–605 (2002).

145. Casellas, P., Galiegue, S., Basile, A.S. Peripheral benzodiazepine receptors and mitochondrial function. Neurochem Int 40, 475–486 (2002).

146. Venneti, S., Lopresti, B.J., Wiley, C.A. The peripheral benzodiazepine receptor (translocator protein 18kDa) in microglia: From pathology to imaging. Prog Neurobiol 80, 308–322 (2006).

147. Campbell. S.J., Zahid, I., Losey, P., et al. Liver Kupffer cells control the magnitude of the inflammatory response in the injured brain and spinal cord. Neuropharmacology 55, 780–787 (2008).

148. Hofman, F.M., Hinton, D.R., Johnson, K., et al. Tumor necrosis factor identified in multiple sclerosis brain. J Exp Med 170, 607–612 (1989).

149. Boka, G., Anglade, P., Wallach, D., et al. Immunocytochemical analysis of tumor necrosis factor and its receptors in Parkinson's disease. Neurosci Lett 172, 151–154 (1994).

150. Hallenbeck, J.M. The many faces of tumor necrosis factor in stroke. Nat Med 8, 1363–1368 (2002).

151. Dickson, D.W. The pathogenesis of senile plaques. J Neuropathol Exp Neurol 56, 321–339 (1997).

152. Campbell, S.J., Jiang, Y., Davis, A.E., et al. Immunomodulatory effects of etanercept in a model of brain injury act through attenuation of the acute-phase response. J Neurochem 103, 2245–2255 (2007).

153. Johnston, B., Burns, A.R., Suematsu, M., et al. Chronic inflammation upregulates chemokine receptors and induces neutrophil migration to monocyte chemoattractant protein-1. J Clin Invest 103, 1269–1276 (1999).

154. Cushing, S.D., Berliner, J.A., Valente, A.J., et al. Minimally modified low density lipoprotein induces monocyte chemotactic protein 1 in human endothelial cells and smooth muscle cells. Proc Natl Acad Sci USA 87, 5134–5138 (1990).

155. Yoshimura, T., Robinson, E.A., Tanaka, S., et al. Purification and amino acid analysis of two human monocyte chemoattractants produced by phytohemagglutinin-stimulated human blood mononuclear leukocytes. J Immunol 142, 1956–1962 (1989).

156. Barna, B.P., Pettay, J., Barnett, G.H., et al. Regulation of monocyte chemoattractant protein-1 expression in adult human non-neoplastic astrocytes is sensitive to tumor necrosis factor (TNF) or antibody to the 55-kDa TNF receptor. J Neuroimmunol 50, 101–107 (1994).

157. Rollins, B.J. JE/MCP-1: an early-response gene encodes a monocyte-specific cytokine. Cancer Cells 3, 517–524 (1991).

158. Lu, B., Rutledge, B.J., Gu, L., et al. Abnormalities in monocyte recruitment and cytokine expression in monocyte chemoattractant protein 1-deficient mice. J Exp Med 187, 601–608 (1998).

159. Hausmann, E.H., Berman, N.E, Wang Y.Y., et al. Selective chemokine mRNA expression following brain injury. Brain Res 788, 49–59 (1998).

160. Song, L., Pachter, J.S. Monocyte chemoattractant protein-1 alters expression of tight junction-associated proteins in brain microvascular endothelial cells. Microvasc Res 67, 78–89 (2004).

161. Tauber, W. Serious adverse effects associated with the use of anti-TNF alpha drugs. Available at http://www.fda.gov. (2005)

162. Selmaj, K.W., Raine, C.S. Experimental autoimmune encephalomyelitis: immunotherapy with anti-tumor necrosis factor antibodies and soluble tumor necrosis factor receptors. Neurology 45, S44–49 (1995).

163. Quang, T.T., Hatem, R., Rousseau, G., et al. Dual effect of pre-ischaemic administration of TNF-alpha on myocardial infarct size. World J Cardio Dis 3, 21–25 (2013).

164. Cross, A., Moots, R.J., Edwards, S.W. The dual effects of TNFα on neutrophil apoptosis are mediated via differential effects on expression of Mcl-1 and Bfl-1. Blood 111, 878–884 (2008).

165. Rancan, M., Otto, V.I., Hans, V.H., et al. Upregulation of ICAM-1 and MCP-1 but not of MIP-2 and sensorimotor deficit in response to traumatic axonal injury in rats. J Neurosci Res 63, 438–446 (2001).

166. Semple, B.D., Bye, N., Rancan, M., et al. Role of CCL2 (MCP-1) in traumatic brain injury (TBI): evidence from severe TBI patients and CCL2-/- mice. J Cereb Blood Flow Metab 30, 769–782 (2010).

167. Lui, S.X., Zhang, Z.G., Zhang, R.L., et al. Chemokine ligand 2 (CCL2) induces migration and differentiation of subventricular zone cells after stroke. J Neurosci Res 85, 2120–2125 (2007).

168. Bode, J.G., Albrecht, U., Haussinger, D., et al. Hepatic acute phase proteins – regulation by IL-6- and IL-1-type cytokines involving STAT3 and its crosstalk with NF-κB-dependent signaling. Eur J Cell Biol 91, 496–505 (2012).

169. Ravetch, J.V. Biochemical characterization of a gamma interferon-inducible cytokine (IP-10). J Exp Med 166, 1084–1097 (1987).

170. Campbell, J.D., Gangur, V., Simons, F.E., et al. Allergic humans are hyporesponsive to a CXCR3 ligand-mediated Th1 immunity-promoting loop. FASEB 18, 329–331 (2004).

171. Vanguri, P. Interferon-gamma-inducible genes in primary glial cells of the central nervous system: comparisons of astrocytes with microglia and Lewis with brown Norway rats. J Neuroimmunol 56, 35–43 (1995).

172. Oh, J.W., Schwiebert, L.M., Benveniste, E.N. Cytokine regulation of CC and CXC chemokine expression by human astrocytes. J Neurovirol 5, 82–94 (1999).

173. Aid, S., Silva, A.C., Candelario-Jalil, E., et al. Cyclooxygenase-1 and -2 differentially modulate lipopolysaccharide-induced blood-brain barrier disruption through matrix metalloproteinase activity. J Cereb Blood Flow Metab 30, 370–380 (2010).

174. Kang, Y.J., Mbonye, U.R., DeLong, C.J., et al. Regulation of intracellular cyclooxygenase levels by gene transcription and protein degradation. Prog Lipid Res 46, 108–125 (2007).

175. Wang, H., Hitron, I.M., Iadecola, C., et al. Synaptic and vascular associations of neurons containing cyclooxygenase-2 and nitric oxide synthase in rat somatosensory cortex. Cereb Cortex 15, 1250–1260 (2005).

176. Choi, S.H., Aid, S., Choi, U., et al. Cyclooxygenases-1 and -2 differentially modulate leukocyte recruitment into the inflamed brain. Pharmacogenomics J 10, 448–457 (2010).

177. Candelario-Jalil, E., Taheri, S., Yang, Y., et al. Cyclooxygenase inhibition limits blood-brain barrier disruption following intracerebral injection of tumor necrosis factor-alpha in the rat. J Pharmacol Exp Ther 323, 488–498 (2007).

178. Chouly, C., Pouliquen, D., Lucet, I., et al. Development of superparamagnetic nanoparticles for MRI: effect of particle size, charge and surface on biodistribution. J Microencapsul 13, 245–255 (1996).

179. Osaka, T., Nakanishi, T., Shanmugam, S., et al. Effect of surface charge of magnetite nanoparticles on their internalization into breast cancer and umbilical vein endothelial cells. Colloids Surf B 71, 325–330 (2009).

180. Moghimi, S.M., Hunter, A.C., Murray, J.C. Long-circulating and target-specific nanoparticles: theory to practice. Pharmacol Rev 53, 283–318 (2001).

181. Lee, H., Yu, M.K., Park, S., et al. Thermally cross-linked superparamagnetic iron oxide nanoparticles: synthesis and application as a dual imaging probe for cancer in vivo. J Am Chem Soc 129, 12739–12745 (2007).

182. Mahmoudi, M., Simchi, A., Imani, M. et al. Optimal design and characterization of superparamagnetic iron oxide nanoparticles coated with polyvinyl alcohol for targeted delivery and imaging. J Phys Chem B 112, 14470–14481 (2008).

183. Liu, H.L., Ko, S.P., Wu, J.H., et al. One-pot polyol synthesis of monosize PVP-coated sub-5 nm Fe_3O_4 nanoparticles for biomedical applications. J Magn Magn Mater 310, 815–817 (2007).

184. Ma, Y.H., Wu, S.Y., Wu, T., et al. Magnetically targeted thrombolysis with recombinant tissue plasminogen activator bound to polyacrylic acid-coated nanoparticles. Biomater 30, 3343–3351 (2009).

185. Xu, F.H., Cheng, C.M., Xu, F.J., et al. Superparamagnetic magnetite nanocrystal clusters: a sensitive tool for MR cellular imaging. Nanotechnology 20, 405102 (2009).

186. He, N., Wang, Z., Li, S. DNA separation and amplification application of (Fe_3O_4/PMMA)/SiO2 nanoparticles with core-shell structure. Abstracts of Papers, American Chemical Society (2006).

187. Ma, D.C., Wasylaschuk, W.R., Beasley, C. et al. Identification and quantitation of extractables from cellulose acetate butyrate (CAB) and estimation of their in vivo exposure levels. J Pharm Biomed Anal 35, 779–788 (2004).

188. Juang, J.H., Shen, C.R., Wang, J.J., et al. Magnetic resonance imaging of transplanted mouse islets labeled with chitosan-coated superparamagnetic iron oxide nanoparticles. Transplant Proc 42, 2104–2108 (2010).

189. Jarrett, B.R., Frendo, M., Vogan, J., et al. Size-controlled synthesis of dextran sulfate coated iron oxide nanoparticles for magnetic resonance imaging. Nanotechnology 18, 35603 (2007).

190. Saboktakin, M., Maharramov, A., Ramazanov, M. Synthesis and characterization of superparamagnetic nanoparticles coated with carboxymethyl starch (CMS) for magnetic resonance imaging technique. Carbo Pol 78, 292–295 (2009).

191. Miltenyi, S., Muller, W., Weichel, W., et al. High gradient magnetic cell separation with MACS. Cytometry 11, 231–238 (1990).

192. Gaihre, B., Khil, M.S., Lee, D.R., et al. Gelatin-coated magnetic iron oxide nanoparticles as carrier system: drug loading and in vitro drug release study. Int J Pharm 365, 180–189 (2009).

193. Li, G.F., Fan, J.D., Jiang, R., et al. Cross-linking the linear polymeric chains in the ATRP synthesis of iron oxide/polystyrene core/shell nanoparticles. Chem Mater 16, 1835–1837 (2004).

194. Emile, J., Laurence, M., Juliette, V., et al. E-selectin as a target for drug delivery and molecular imaging. J Cont Release 158, 194–206 (2012).

195. Zhang, Y., Kohler, N., Zhang, M.Q. Surface modification of superparamagnetic magnetite nanoparticles and their intracellular uptake. Biomaterials 23, 1553–1561 (2002).

196. Mahmoudi, M., Shokrgozar, M.A., Simchi, A., et al. Multiphysics flow modeling and in vitro toxicity of iron oxide nanoparticles coated with poly(vinyl alcohol). J Phys Chem C 113, 2322–2331 (2009).

197. Mahmoudi, M., Simchi, A., Imani, M., et al. An in vitro study of bare and poly-(ethylene glycol)-co-fumarate-coated superparamagnetic iron oxide nanoparticles: A new toxicity identification procedure. Nanotechnology 20, 225104 (2009).

198. Chorny, M., Polyak, B., Alferiev, I.S., et al. Magnetically driven plasmid DNA delivery with biodegradable polymeric nanoparticles. FASEB 21, 2510–2519 (2007).

199. Huang, G., Diakur, J., Xu, Z., et al. Asialoglycoprotein receptor-targeted superparamagnetic iron oxide nanoparticles. Int J Pharm 360, 197–203 (2008).

200. Muller, K., Skepper, J.N., Posfai, M., et al. Effect of ultrasmall superparamagnetic iron oxide nanoparticles (Ferumoxtran-10) on human monocyte-macrophages in vitro. Biomaterials 28, 1629–1642 (2007).

201. Babic, M., Horok, D., Jendelov, P., et al. Poly(N,N-dimethylacrylamide)-coated maghemite nanoparticles for stem cell labeling. Bioconjugate Chem 20, 283–294 (2009).

202. Hussain, S.M., Hess, K.L., Gearhart, J.M., et al. In vitro toxicity of nanoparticles in BRL 3A rat liver cells. Toxicol 19, 975–983 (2005).

203. Mahmoudi, M., Simchi, A., Vali, H., et al. Cytotoxicity and cell cycle effects of bare and poly(vinyl alcohol)-coated iron oxide nanoparticles in mouse fibroblasts. Adv Eng Mater 11, 243–250 (2009).

204. Mahmoudi, M., Simchi, A., Imani, M. Cytotoxicity of uncoated and polyvinyl alcohol coated superparamagnetic iron oxide nanoparticles. J Phys Chem C 113, 9573–9580 (2009).

205. Kamei, K., Mukai, Y., Kojima, H., et al. Direct cell entry of gold/iron-oxide magnetic nanoparticles in adenovirus mediated gene delivery. Biomaterials 30, 1809–1814 (2009).

206. Karlsson, H.L., Cronholm, P., Gustafsson, J., et al. Copper oxide nanoparticles are highly toxic: A comparison between metal oxide nanoparticles and carbon nanotubes. Chem Res Toxicol 21, 1726–1732 (2008).

207. Lynch, I. Are there generic mechanisms governing interactions between nanoparticles and cells? Epitope mapping the outer layer of the protein-material interface. Physica A 373, 511–520 (2007).

208. Nel, A.E., Madler, I., Velegol, D., et al. Understanding biophysicochemical interactions at the nano-bio interface. Nat Mater 8, 543–557 (2009).

209. Lynch, I., Cedervall, T., Lundqvist, M., et al. The nanoparticle-protein complex as a biological entity; a complex fluids and surface science challenge for the 21st century. Adv Colloid Interface Sci 134–135, 167–174 (2007).

210. Weissleder R, Elizondo G, Wittenberg J, et al. Ultrasmall superparamagnetic iron oxide: characterization of a new class of contrast agents for MR imaging. Radiology 175, 489–493 (1990).

211. Saleh, A., Wiedermann, D., Schroeter, M., et al. Central nervous system inflammatory response after cerebral infarction as detected by magnetic resonance imaging. NMR Biomed 17, 163–169 (2004).

212. Saleh, A., Schroeter, M., Ringelstein, A., et al. Iron oxide particle-enhanced MRI suggests variability of brain inflammation at early stages after ischaemic stroke. Stroke 38, 2733–2737 (2007).

213. Vellinga, M.M., Oude Engberink, R.D., Seewann, A., et al. Pluriformity of inflammation in multiple sclerosis shown by ultra-small iron oxide particle enhancement. Brain 131, 800–807 (2008).